



Fisheries and Oceans
Canada

Pêches et Océans
Canada

Ecosystems and
Oceans Science

Sciences des écosystèmes
et des océans

Canadian Science Advisory Secretariat (CSAS)

Research Document 2022/021

Maritimes Region

Optical, Chemical, and Biological Oceanographic Conditions in the Labrador Sea between 2014 and 2018

M. Ringuette, E. Devred, K. Azetsu-Scott, E. Head, S. Punshon, B. Casault, and S. Clay

Ocean and Ecosystem Sciences Division, Science Branch
Department of Fisheries and Oceans
Bedford Institute of Oceanography
P.O. Box 1006, 1 Challenger drive
Dartmouth, Nova Scotia B2Y 4A2

Foreword

This series documents the scientific basis for the evaluation of aquatic resources and ecosystems in Canada. As such, it addresses the issues of the day in the time frames required and the documents it contains are not intended as definitive statements on the subjects addressed but rather as progress reports on ongoing investigations.

Published by:

Fisheries and Oceans Canada
Canadian Science Advisory Secretariat
200 Kent Street
Ottawa ON K1A 0E6

[http://www.dfo-mpo.gc.ca/csas-sccs/
csas-sccs@dfo-mpo.gc.ca](http://www.dfo-mpo.gc.ca/csas-sccs/csas-sccs@dfo-mpo.gc.ca)



© Her Majesty the Queen in Right of Canada, 2022
ISSN 1919-5044
ISBN 978-0-660-42801-7 Cat. No. Fs70-5/2022-021E-PDF

Correct citation for this publication:

Ringuette, M., Devred, E., Azetsu-Scott, K., Head, E., Punshon, S., Casault, B. and Clay, S.
2022. Optical, Chemical, and Biological Oceanographic Conditions in the Labrador Sea
between 2014 and 2018. DFO Can. Sci. Advis. Sec. Res. Doc. 2022/021. v + 38 p.

Aussi disponible en français :

*Ringuette, M., Devred, E., Azetsu-Scott, K., Head, E., Punshon, S., Casault, B., et Clay, S.
2022. Conditions océanographiques optiques, chimiques, et biologiques dans la mer du
Labrador entre 2014 et 2018. Secr. can. des avis sci. du MPO. Doc. de rech. 2022/021.
v + 40 p.*

TABLE OF CONTENTS

ABSTRACT	v
INTRODUCTION	1
DATA SOURCES AND METHODS OF ANALYSIS	2
<i>IN SITU</i> SAMPLES COLLECTION.....	2
Core stations	2
Biological stations	3
DISCRETE VARIABLE MEASUREMENTS AND DATA COLLECTION	3
Transient Tracers SF ₆ and CFC-12.....	3
pH Measurements.....	4
Total Inorganic Carbon (TIC) and Total Alkalinity (TA)	4
Discrete pCO ₂	4
Surface temperature (Surface to 100 m).....	5
Nutrients.....	5
<i>In situ</i> Chlorophyll-a concentration.....	6
Satellite-derived Chlorophyll-a concentration.....	6
Mesozooplankton	6
Continuous Plankton Recorder Data.....	7
COMPUTATIONAL METHODS	8
Vertical binning.....	8
Scorecards	8
Spring bloom metrics	8
Access to Data Products.....	9
RESULTS AND DISCUSSION	9
TOTAL INORGANIC CARBON AND PH	9
TRANSIENT TRACERS CFC-12 AND SF ₆	10
TEMPERATURE IN THE TOP 100 M.....	10
NUTRIENTS.....	11
<i>IN SITU</i> CHLOROPHYLL-A CONCENTRATION.....	11
SATELLITE-DERIVED SPRING BLOOM INDICES.....	12
MESOZOOPLANKTON.....	12
CONTINUOUS PLANKTON RECORDER	13
Phytoplankton	13
Mesozooplankton	14
Macrozooplankton.....	14
Acid sensitive taxa	14
SUMMARY.....	14
ACKNOWLEDGEMENTS	15
REFERENCES CITED.....	16

TABLES	19
FIGURES	20
ANNEX 1.....	35

ABSTRACT

The chemistry and biology of the Labrador Sea and adjacent shelves have undergone significant changes over the 2014–2018 period compared to previous years. The Atlantic Zonal Off-shelf Monitoring Program (AZOMP) revealed an increase in dissolved inorganic carbon and a decrease in pH, a trend that extends back to the beginning of the monitoring program in the mid-1990s. While the mean concentration of chlorofluorocarbon (CFC-12) over the water column has remained stable, the concentration of sulfur hexafluoride (SF₆) has been increasing steadily since we began to measure it in 2011, reflecting the atmospheric history of these gasses. The mean temperature of the top layer (0–100 m) has been mainly below normal since 2011, except for the Labrador Shelf where two warmer-than-normal years were observed in 2015 and 2018. The lower-than-normal temperatures were associated with higher-than-normal nutrient concentrations in the same layer. The timing of the cruise, which tend to become earlier than usual because of constrained crew change dates, can partly explain these findings and point out the need for consistent dates in sea-going expeditions to remove uncertainties related to sampling time. Deep nutrients exhibited inter-annual variations up until 2014, and mostly remained above average today. Since 2014, both phytoplankton (as indicated by chlorophyll-a concentration) and mesozooplankton abundances have remained below the 1999–2010 average in all three regions of interest: the Labrador Shelf, the Labrador Central Basin, and the Greenland Shelf. Plankton monitoring by means of the Continuous Plankton Recorder (CPR) has been carried out in the northwest Atlantic since the early 1960s. In 2017 (the most recent data available), three indicators of phytoplankton biomass showed high values in the region adjacent to the Newfoundland Shelf (40°W to 45°W) compared with previous years/decades. This was also the case for the abundances of six out of seven mesozooplankton taxa. Further east, one of the phytoplankton color index and six of the seven mesozooplankton taxa showed positive anomalies in 2017. The abundance of one macrozooplankton taxon (Hyperiid amphipods) has increased throughout the northwest Atlantic over all sampling decades/years, while that of a second taxon (Euphausiids) has decreased. The abundances of three acid-sensitive taxa in 2017 were all higher than the 1990–2009 average throughout the sub-polar gyre and on the Newfoundland Shelf.

INTRODUCTION

The Labrador Sea is a deep basin nested between Labrador and Greenland with a cyclonic circulation pattern that leads to the mixing of Arctic and North Atlantic water. The Baffin Island and Labrador currents transport cold and less-saline Arctic water southward along the Canadian coast (Wang et al. 2016). On the eastern side, the West Greenland Current brings warmer, more-saline waters northward, along the Greenland coast into the Baffin Bay, where it meets the Labrador Current. (See Lozier et al. 2019 and Yashayaev et al. 2017 for a detailed description of the Labrador Sea Circulation.) By the end of winter, the cooling of the upper layer results in an increase of surface density, enabling wind-driven mixing to reach greater depths (1,500 to 2,000 m), thus ventilating the deeper ocean with atmospheric gases while pumping nutrients from the deep waters to the surface. The intensity of this phenomenon varies with environmental factors, including atmospheric forcing, freshwater runoff from adjacent glaciers, precipitation, intrusion of warm and saline inflow from the adjacent North Atlantic, and intrusion of cold and fresh water from the Arctic Ocean. In turn, this deep mixing strongly impacts heat flux, stratification, and by extension, the chemical balance and biological productivity of the Labrador Sea. Consequently, changes in the physical and chemical environment of the aphotic zone influence both plankton community composition and annual biological production cycles, including fish and higher trophic level.

About one quarter of carbon dioxide (CO₂) released by human activities is taken up by the oceans (Sabine et al. 2004), altering ocean chemistry, and correspondingly, the marine carbonate system. The Labrador Sea hosts a strong “solubility pump”, whereby anthropogenic CO₂ sequestered from the atmosphere is transported to the deep ocean by chemical and physical processes. The dissolution of anthropogenic CO₂ has decreased ocean pH by 0.1 units over the past 200 years, corresponding to a 30% increase in acidity (Caldeira and Wickett 2003). If global emissions of CO₂ remain at their present rate, ocean pH is predicted to drop by an additional 0.3 units by 2100. The oceans have not experienced such a rapid pH decrease (ocean acidification), or one of such a high magnitude, for at least 20 million years (Feely et al. 2004), raising serious concerns about the ability of marine ecosystems to adapt. The major impact of decreasing pH will be felt by organisms that form calcium carbonate (CaCO₃) shells and skeletons, because rising acidity increases the solubility of CaCO₃. Since CaCO₃ shells and skeletons are naturally more soluble at lower temperatures and higher pressures, high latitudes and deep water ecosystems, such as the one encountered in the Labrador Sea, are more vulnerable to the added stress of ocean acidification than those at intermediate latitudes. Furthermore, rapid environmental changes, such as receding sea-ice extent and enhanced hydrological cycles, may amplify these problems. Inert halogenated trace gases of anthropogenic origin that have accumulated in the atmosphere, such as the chlorofluorocarbons (CFCs) and sulfur hexafluoride (SF₆), are used to study ventilation and transport processes in the ocean. In recent decades, they have been used to calculate Transient Tracer Distribution (TTD) to estimate the transit time of water masses and anthropogenic CO₂ in the water (Haine and Hall 2002, Hall et al. 2002).

Since 1990, as part of the World Ocean Circulation Experiment (WOCE), the Ocean and Ecosystem Sciences Division (OESD) at the Bedford Institute of Oceanography (BIO) has carried out an annual occupation, usually in the spring, of the AR7W (Atlantic Repeat Hydrography Line 7 West) oceanographic section across the Labrador Sea (Figure 1). Soon after its inception, the program morphed into Fisheries and Oceans Canada (DFO) Atlantic Zone Off-shelf Monitoring Program (AZOMP), following the OESD’s overarching objectives to: 1) characterize and understand the causes of ocean variability at seasonal, inter-annual, and inter-decadal scales; 2) provide adequate data to monitor the health of the marine ecosystem

and support decision-making based on scientific evidence; and 3) to build historical databases to address future issues. The program also contributes to the international Global Climate Observing System (GCOS) and the Climate Variability (CLIVAR) component of the World Climate Research Program (WCRP) and it reports annually with an environmental synopsis to the Northwest Atlantic Fisheries Organization (NAFO).

The AR7W section spans approximately 900 km across the southern edge of the Labrador Sea, from the Labrador Shelf (near 53°N) to the Greenland Shelf (near 61°N) (Figure 1). The annual AZOMP multidisciplinary survey of the Labrador Sea primarily consists of AR7W occupations and deployments/recoveries of moorings and Argo floats. The ideal timing of the mission in May aims to capture the fading winter-deep-convection signal and the beginning of the phytoplankton bloom and productivity season, while avoiding possible sea-ice on the Labrador Shelf early in the spring. Inter-annual variability in the spring bloom makes the sampling of the spring bloom uncertain, with early cruise dates in recent decades often falling ahead of the bloom (Table 1; Figure 2). With nearly three decades of measurements, the time series allows examination of decadal trends in all key ecosystem variables (i.e., temperature, plankton biomass, and abundance).

In the Labrador Basin, light limits primary production for most of the year (Harrison and Li 2008, Fragoso et al. 2016), while a shallow mixed layer and relatively low nitrate concentration limit phytoplankton growth on the Labrador Shelf. Phytoplankton growth also seemed to be limited by availability of silicate in the Central Labrador Basin (Harrison and Li 2008). These conditions support the emergence of small flagellates such as *Phaeocystis pouchetii* in the northern and eastern region of the Labrador Sea, which can form massive blooms under favorable conditions (Fragoso et al. 2016). The Labrador Shelf, influenced by Arctic waters, is dominated by polar diatom species (*Thalassiosira* spp. and *Bacteriosira bathyomphala*) and species associated with sea-ice (*Porosira glacialis* and *Fossula arctica*). Primary production patterns and mesoscale features leave their imprint on the mesozooplankton distribution and abundance (Yebra et al. 2009). One species of copepod, *Calanus finmarchicus*, dominates the mesozooplankton biomass throughout the central region of the Labrador Sea, while on the shelves, two Arctic *Calanus* species, *C. glacialis* and *C. hyperboreus*, are equally important (Head et al. 2003). *C. finmarchicus* abundance shows regional variations that are generally consistent from year-to-year and are related to differences in the timing of life-cycle events, which are influenced by environmental conditions, including spring bloom dynamics.

This report describes the biogeochemical state of the Labrador Sea from 2014 to 2018. Data presented in this report come from: 1) annual surveys carried out over 2-week periods, between early May and early August; 2) satellite remote-sensing of daily observations of ocean colour, compiled into semi-monthly spatial averages; and 3) the Continuous Plankton Recorder (CPR) survey that collects monthly samples along commercial shipping routes and that are spatially averaged.

DATA SOURCES AND METHODS OF ANALYSIS

The following section describes the data sources and sampling methods used for the estimation of the biogeochemical variables and indices depicted in the present report.

***IN SITU* SAMPLES COLLECTION**

Core stations

The core stations remain the priority of the monitoring program to ensure geographical consistency over time when reporting on the data. The main goal of the sampling is to obtain a

complete suite of measurements at selected locations from surface to bottom to characterize the physical and chemical properties of the entire water column and the biological properties in the upper layers. The CTD-rosette system used to carry out measurements and water collection includes twelve 24 L Niskin bottles and a core of twinned sensors to measure temperature, salinity and oxygen, as well as additional sensors to measure fluorescence, pH, light attenuation, Photosynthetically Active Radiation (PAR), absorption by Colored Dissolved Organic Matter (CDOM), and current velocity (LADCP). Water samples are collected in the top 150 m at depths of 5 m, 25 m, 50 m, 100 m, and 150 m to measure transient gases (CFC and SF₆), oxygen, partial pressure of carbon dioxide (pCO₂), Total Inorganic Carbon (TIC), alkalinity, pH, nutrients, salinity, chlorophyll-a, and phytoplankton accessory pigments concentration. Once the CTD-Rosette is onboard, the collection of water from the Niskin bottles is carried out as listed previously (i.e., gases first and phytoplankton last) to minimize the loss of transient tracers and other gases during sampling. All variables were sampled and analyzed following GO-SHIP protocols (Hood et al. 2010, Mitchell et al. 2002). In addition to water sampling from the Niskin bottles, mesozooplankton are collected in vertical net hauls in the upper 100 m using a 0.75 m diameter ring net fitted with a 200 µm mesh, and 0.5 m diameter ring net with a 76 µm mesh size. A detailed description of the processing of the physical oceanographic data is presented in Yashayaev et al. 2020.

When time allows, extra stations are added between core stations in order to increase the spatial resolution of the sampling. However, on these stations only measurements from the sensors located on the CTD-Rosette are recorded and water is not collected unless requested by programs outside the core program. At these stations, the CTD-Rosette system is lowered to the bottom to profile the entire water column. Note that in the current report, only data collected on the core and biological stations are included.

Biological stations

The purpose of these stations is to increase the vertical resolution compared to core stations and to carry out Photosynthesis-Irradiance (P-I) 14C-uptake experiments with phytoplankton (water) samples. In these experiments, 33 aliquots of phytoplankton from two depths (surface and close to the deep chlorophyll-a maximum) are incubated with 14C -bicarbonate at in situ temperatures and 30 light levels (+ 3 dark bottles) for approximately 3 hours. The P-I measurements are used to estimate primary production according to Platt and Jassby (1976). The actual location of the biological stations is not critical, so the vessel is stopped mid-morning wherever we are transiting between stations, in order to begin, the incubations can start around noon, local time, for the consistency of the method. Because the biological stations focus on the upper layers of the water column, the Conductivity, Temperature, Depth (CTD) sensor is only lowered to 200 m, allowing for a greater vertical resolution of all the biogeochemical parameters. Bottles are closed at 2 m, 10 m, 20 m, 30 m, 40 m, 50 m, 60 m, 80 m, 100 m, and 150 m, with an extra bottle at the depth of the deep chlorophyll-a maximum, as revealed by the in situ fluorescence sensor. A total of seven biological stations are sampled, which are spread along the AR7W transect: two on the Labrador Shelf, three in the Central Labrador Basin, and two on the Greenland Shelf.

DISCRETE VARIABLE MEASUREMENTS AND DATA COLLECTION

Transient Tracers SF₆ and CFC-12

Prior to analysis, seawater samples from the rosette were drawn directly into 250 mL glass syringes and were stored at approximately 4 °C in a low-temperature incubator for up to 12 hours. Immediately before analysis, the samples were warmed to approximately 20 °C in a

water bath then injected into the purge vessel of a custom-made purge-and-trap system, where dissolved gases were stripped from the sample in a stream of ultra-high-purity nitrogen with a flow rate of 140 mL per minute. The SF₆ and CFC-12 gases were quantitatively retained in a trap comprised of 30 cm of 1/16" stainless steel tubing packed with 100–120 mesh Carboxen 1,000, held at -70 °C over liquid nitrogen. After each 7 minute purge cycle, the trap was heated to 180 °C with a low-voltage electric current and the desorbed gases directed to a Varian gas chromatograph equipped with an electron-capture detector. SF₆ and CFC-12 were separated on a one-meter pre-column packed with Porasil B and a three-meter main column packed with Molecular Sieve 5A held isothermally at 100 °C. Total run-time was 11.5 minutes. The chromatographic sample peaks were quantified with Varian Galaxie software and the analytical system calibrated at least once each day using an air standard supplied by the Climate Monitoring and Diagnostics Laboratory of the National Oceanic and Atmospheric Administration (CMDL/NOAA), Boulder, Colorado. Analytical precision, as determined by repeated standard injections, was around ± 2% for SF₆ and ± 0.7% for CFC-12.

pH Measurements

Seawater was analyzed for pH according to spectrophotometric Standard Operating Procedure 6b (SOP 6b) described in *Guide to best practices for ocean CO₂ measurements* (Dickson et al. 2007). Water was collected from the rosette in 60 mL borosilicate glass tubes, allowing each sample to overflow by at least one volume. Samples were stored in a low-temperature incubator at 4 °C prior to analysis. The maximum time between sampling and analysis was about 4 hours. Racks of tubes were then placed in a water bath held at 25 °C and allowed to thermally equilibrate for 30 minutes. Each sample was then introduced into a water-jacketed 10 cm quartz cell and 30 µL of the purified indicator dye m-cresol purple added before mixing well. The absorbance of light at the wavelengths 434 and 578 nm was measured with an Agilent photodiode array spectrophotometer and the resulting extinction coefficients at these wavelengths were used to determine the pH of the sample. The performance of the spectrophotometer was monitored by daily measurements of a trisaminomethane (Tris) buffer solution of known pH.

Total Inorganic Carbon (TIC) and Total Alkalinity (TA)

Seawater samples were collected in 500 mL borosilicate glass bottles and preserved with mercuric chloride following the method described in *Guide to best practices for ocean CO₂ measurements* (Dickson et al. 2007). Total Inorganic Carbon (TIC) was later determined using gas extraction and coulometric titration with photometric endpoint detection (Johnson, et al. 1987). Total Alkalinity (TA) was measured by open-cell potentiometric titration with full curve Gran Point determination using a Titrandosimat with Tiamo software, in conjunction with a sample-delivery system built in-house. Certified Reference Material (CRM) (supplied by Professor Andrew Dickson, Scripps Institution of Oceanography, San Diego, USA) was analyzed in duplicate at intervals to calibrate for accuracy.

Discrete pCO₂

Water samples for pCO₂ measurements were drawn from the rosette (following dissolved oxygen) into 160 mL volume crimp seal vials, allowing each sample vial to overflow by about 3 volumes before immediately preserving with 50 µL of saturated mercuric chloride solution and crimp sealing with butyl rubber septa. The samples were stored at 4 °C and analyzed at BIO's chemical laboratory upon return. Surface samples were collected at every station throughout the cruise and two full-depth profiles were collected from Stations 17 and 18 on the AR7W line.

pCO₂ was later determined by headspace equilibrium gas chromatography with flame ionization detection, using the method of Neill et al. (1997).

Surface temperature (Surface to 100 m)

Conductivity, Temperature, Depth (CTD) profiles are collected between the surface and near bottom (often several thousand meters deep), however, in this section we report only on temperature collection from the 0–100 m range, which are the most relevant for our biological sampling. (See Yashayaev et al. 2020 for full depth hydrography) CTD profiles are binned at 1 m resolution and the arithmetic average is computed to provide the single temperature values for the 0–100 m layer. The first few meters from the downward casts are generally not recorded, due to the requirement for an underwater acclimation period for the sensors at-depth, which is performed first. Following the acclimation period, the instrument is brought as close as possible to the surface but, partly because of the ship's movements, the sensors do not reach the theoretical 0 m depth. Surface values are obtained by linear extrapolation of the temperatures at the two depths closest to the surface and this value is included in the mean temperature.

Nutrients

Nutrient measurements were made using a SEAL Analytical continuous-flow AutoAnalyzer 3 (AA3) and concentrations are expressed in micromoles per liter. The analytical methods have been modified from the historically used Technicon II: Technicon for Seawater Analysis (Silicate 186 72W, Phosphate 155 71W, Nitrate/Nitrite 158 71W) (K  rouel and Aminot 1997) so as to remain compatible with methods described in the nutrient section of *The GO-SHIP Repeat Hydrography Manual* (Becker et al. 2019). Duplicate nutrient samples were drawn into 10 ml collection vials directly from the rosette without using tubing, with technicians wearing vinyl gloves to avoid contamination. Samples were stored at 4   C and analyzed within 12 hours. Five dissolved inorganic nutrients were analyzed, namely, nitrate plus nitrite (NO₃ + NO₂), nitrite (NO₂), phosphate (PO₄), silicate (SiO₄), and ammonium (NH₄).

The instrument was calibrated for every analytical run, using a six-point calibration curve from pre-made solutions diluted using artificial seawater of same salinity as the samples, distributed over the concentration range for each nutrient. The analysis was followed by a drift standards analysis and blank samples to determine the method's detection limits. The baseline was re-assessed every 12 sample duplicates (i.e., every 6 samples). The pH of the imidazole buffer was monitored to ensure optimal pH levels for the nitrate plus nitrite analyses, and adjusted as needed using hydrochloric acid, thus improving the lifespan and stability of the cadmium reduction column. Ultimately, it diminished drift issues observed in the past between analytical runs.

The quality of these analyses were validated by analyzing a CRM for nutrients produced by KANSO Co., Ltd., Japan. There is no existing reference material for ammonium in seawater, although CRM values were tracked for consistency. In addition to the external quality control validation, an internal validation was implemented through the use of a check (tracking) sample consisting of two litres of water collected from the bottom (at a depth of approximately 500 m) of the Laurentian Channel in the Gulf of Saint Lawrence (LC_01/transit station) and preserved with mercuric chloride (200   L). Aliquots of this sample were measured multiple times during analytical runs throughout the cruise, and results were normalized at the end of the mission. Results from each run were adjusted by the ratio of value for the internal validation on that run, to the mean value for the whole cruise.

***In situ* Chlorophyll-a concentration**

Phytoplankton biomass is represented by the concentration of its main pigment, chlorophyll-a, which was measured using Turner fluorometry (Yentsch and Menzel 1963). Details of the protocol and method can be found in Mitchell et al. (2002). In brief, two replicates of 100 ml aliquots of seawater were drawn from each sampling depth and filtered via vacuum filtration onto 25 mm glass fiber filters (GF/F). The GF/Fs were immediately deposited into separate scintillation vials containing 10 ml of 90% acetone, which were kept at -20 °C for at least 24 hours to ensure extraction of all the chlorophyll-a pigments. Following the extraction period, the aliquots were warmed to room temperature and transferred into fluorometer cuvettes (glass test tubes). The extracts were exposed to blue light (excitation wavelengths) in the fluorometer, which leads them to emit red light. This red light is detected and quantified by a photomultiplier (Holm-Hansen et al. 1965). Chlorophylls other than chlorophyll-a (e.g., chlorophyll-b, chlorophyll-c1, -c2, and -c3) can contribute to the overall fluorescence signal, but their contribution is generally minor. Chlorophyll-a degradation products (a-type phaeopigments associated with senescent phytoplankton or zooplankton fecal pellets) may sometimes be present in a sample and contribute to the fluorescent signal. To account for their contribution, after taking the first fluorescence measurement, samples were acidified, which converts chlorophyll-a into phaeophytin-a. A conversion factor was then applied to retrieve the concentrations of both the chlorophyll-a and a-type phaeopigments (Welschmeyer 1994).

Satellite-derived Chlorophyll-a concentration

In addition to in situ measurements, chlorophyll-a concentrations were derived using satellite ocean colour. This mode of observation provides information on phytoplankton biomass at synoptic scales and daily frequency (assuming clear skies). These satellite-derived data are used to complement the in-situ observations by providing context to the seagoing missions, including a suite of metrics to characterize the phytoplankton spring bloom (see section 4.12). Satellite data presented in this document are retrieved using the MODerate Resolution Imaging Spectroradiometer (MODIS) on the Aqua platform launched by the National Aeronautic Space Administration (NASA) in 2002. While NASA has launched several satellites since 1998, in this report only data from the MODIS sensor are presented in order to have a consistent and climate-compatible time series of chlorophyll-a concentrations that is free of satellite inter-calibration issues. MODIS is the satellite with the longest continuous time series—the first full year of data was 2003 and it is still operating.

For this report, global daily level-3 data at 4 km resolution were downloaded from [NASA Ocean Biology Processing Group](#) and data were extracted for the three regions of interest, namely, the Labrador Shelf (-55.7°E to -53.7°E and 53.6°N to 55.5°N), the Central Basin (-53.7°E to -48.8°E and 55.5°N to 60.1°N), and the Greenland Shelf (-48.8°E to -48.1°E and 60.1°N to 60.7°N) (Figure 1). Chlorophyll-a concentration was retrieved using a band-ratio algorithm (OC3M) that has been modified to correct a known bias at low chlorophyll-a concentration (< 0.15 mg m⁻³, [OceanColor Web](#)). All data are stored at BIO on an ftp server and are made available to public upon email request to emmanuel.devred@dfo-mpo.gc.ca.

Mesozooplankton

Mesozooplankton were collected in vertical net hauls in the upper 100 m, where we find 95% of the biomass in spring-summer (Astthorsson and Gislason 2003), using a 0.75 m diameter ring net fitted with a 200 µm mesh size and 0.5 m diameter ring net with a 76 µm mesh size. The cod-end was attached via a clamp to a weighted hydro-wire and the towing bridle was attached to a crossbow mounted on the wire, at a height above the cod-end such that the net was held vertically. In this configuration, zooplankton were only collected as the net was towed upwards.

The towing speed was about 0.5 m s^{-1} and the volume of water sampled was assumed to be the volume of the cylinder sampled by the net, until 2010, when the filtered volumes started to be measured using a Danemark K/C flowmeter. The flowmeter was equipped with a back-spin pin, to prevent the impeller from spinning during the descent of the net, so that it only measured flow during the ascent. Samples were preserved in 2% formalin. For *C. finmarchicus*, *C. hyperboreus*, and *C. glacialis*, specimens were identified and enumerated to the level of species and stage, and size-frequency distributions of sizes-at-stage were constructed for all stages at each station. Other taxa were identified to the level of species (sometimes to stage), genus, or group, depending on their abundance in the samples. Meaningful abundances were obtained when a minimum of 300 organisms, and a minimum of 200 *Calanus* spp., were counted to allow assessment of community structure and *Calanus* population growth/development, respectively.

Continuous Plankton Recorder Data

The Continuous Plankton Recorder (CPR) is an instrument towed by commercial ships that collects plankton at a depth of about 7 m on a long continuous ribbon of silk (approximately 260 μm mesh). The position on the silk, together with information on the timing/position of CPR deployment, provides information on the sample location. CPR data were analyzed to detect changes in indices of phytoplankton concentration (colour and relative numerical abundance) and zooplankton relative abundance for different months, years and/or decades. The indices indicated relative changes in concentration (Richardson et al. 2006). The sampling methods from the first surveys in the northwest Atlantic (early 1960s) to the present were identical so that valid comparisons can be made between months, years, and decades. CPR data collected from January to December in a given year are made available to the DFO data archive two years later (on January of that year).

The tow routes between Reykjavik and the Gulf of Maine were divided into eight regions: the Western Scotian Shelf (WSS), the Eastern Scotian Shelf (ESS), the South Newfoundland Shelf (SNS), the Newfoundland Shelf (NS), and four regions in the northwest Atlantic sub-polar gyre, divided into bins of 5 degrees of longitude (Figure 3). In this report, a broad-scale comparison is presented for CPR data collected in all regions and all sampling decades. More detailed analyses for the Scotian Shelf and Newfoundland Shelf regions are presented in the annual AZMP Reports from the Maritimes and Newfoundland regions.

Monthly average abundances ($\log_{10}[N+1]$) transformed for all but Phytoplankton Colour Index (PCI) were calculated for 15 CPR taxa by averaging values for all individual samples collected within each region for each month and year. These regional monthly average abundances were further averaged by month for samples collected within each decade prior to 2009, (i.e., 1960–1969, 1970–1979, 1980–1989, 1990–1999, and 2000–2009) to provide decadal monthly-average abundances. The latter were then averaged over each decade to give decadal annual-average abundances. During the 1980s, sampling was too infrequent to calculate decadal annual-average abundances, except for the three regions between 30°W and 45°W, although these regions were also missing sampling in January and December. The averages of the monthly values for the 1970s and 1990s were used to fill in these missing months, so that decadal annual-average abundances could be calculated for all decades. The averages of the decadal annual-average abundances over the 4 or 5 sampling decades represent the climatological annual abundances. Four-year, annual-average abundances were calculated for 2010–2016, using the monthly averages, and annual-average abundances were calculated for 2017, when possible. In this analysis, annual averages for individual years were only calculated if there was sampling in more than 8 months, with no gaps of more than 2 consecutive months (linear interpolation being used to fill in for missing months). These criteria were met in 7 of 8 regions in 2017—no annual average abundances could be calculated for the SNS region.

Standardized abundance anomalies were calculated for the decadal (1960s, 1970s, 1980s, 1990s, 2000s), seven-year (2010–2016), and annual (2017) average abundances, by subtracting the climatological average-annual abundances for each time period and dividing by the standard deviations calculated for the annual-average abundances available for the individual years between 1992 and 2009. Given the good sampling coverage over this period, the annual averages were calculated for 13 to 15 individual years out of 18 years in all regions. The underlying assumption of this approach to the calculation of the standardized-abundance anomalies was that inter-annual variability is similar for all decades.

COMPUTATIONAL METHODS

Vertical binning

All temperatures, nutrients, and chlorophyll-*a* concentrations were averaged over selected depth ranges, namely, chl-*a* from 0 to 100 m, surface nutrients from 0 to 100 m and deep nutrients from the first depth below 100 m to bottom. Averaging these properties was chosen over integration to avoid dominance by the large inventories of deep nutrients, given their occurrence over depth ranges of up to 3000 m. Zooplankton values correspond to the integrated abundances in the water column (0–100 m) since collection was carried out using vertical net tows. (See Section 4.9.)

Scorecards

Annual anomalies were calculated as the deviation of an individual year from the mean of the annual estimates over a reference period (1999–2010), and expressed either in absolute units or as normalized quantities (i.e., by dividing by the standard deviation of the annual estimates over the same period).

Scorecards for temperature, surface (0–100 m), and deep (100+ m to bottom) nutrients, chlorophyll-*a* concentration, and mesozooplankton abundance were computed for each region by subtracting the reference mean for this region (i.e., mean between 1999 and 2010 for all variables except 2003–2010 for satellite metrics) from the value for a given year (i.e., annual mean) and dividing by the standard deviation for the reference method:

$$A_y = (M_y - M_r) / (\sigma)$$

where A_y is the anomaly for a given property in a given year (y) and region, M_y is the annual mean, M_r is the reference period mean and σ is the standard deviation for the reference period. This method was selected because it provides good estimates of anomalies and trends for data with large gradients and gaps (Jones and Hulme 1996).

Spring bloom metrics

The arithmetic mean, median, and standard deviation of chlorophyll-*a* concentration for each daily L3 image were computed for the three regions of interest. These basic statistics were computed from raw data without any transformation. While several methods have been developed to characterize the spring bloom, the shifted Gaussian approach (Zhai et al. 2011) has been preferred given its ability to deal with missing data, and it also provided the highest proportion of successful fits compared to other methods such as the threshold or rate of

change¹. Bloom indices were derived using a modified version of the Zhai et al. (2011) model. In this model, a shifted Gaussian is applied to the daily time series for each year to retrieve four metrics that describe the start, duration, magnitude (surface area under the Gaussian curve), and amplitude of the bloom (maximum chlorophyll-a concentration minus the background value). Here, time was expressed in days, referred to as day of year, and counted from the 1st of January of each year. The procedure was carried out in an automatic manner using an optimization function, `nls()`, coded in R, and a visual inspection of each fit was carried out for each year and region to identify abnormal results (e.g., very high chlorophyll-a concentration, i.e., > 30 mg m⁻³ in late spring that lead to very late bloom initiation). Episodic phytoplankton blooms occur at various times of the year including winter and summer. These “secondary” blooms can have an impact on the ability to estimate the peak of the spring bloom, to fit the Gaussian curve and estimate the spring phytoplankton bloom parameters, in particular when more data are available during summer than spring. To ensure that the first large sustained bloom defined as the “spring” bloom was well characterized, we restricted the first half of the shifted Gaussian curve (i.e., initiation to peak) to day of year 110 to 205 for any given year. Phytoplankton growth is short lived (a few days to a week) and spatial distribution is patchy (Denman and Platt 1975), which can make it challenging to estimate spring-bloom dynamics using satellite observations in areas such as the Labrador Sea, where skies are frequently cloudy. Defining regions of interest for satellite observations represents, therefore, a trade-off between selecting small areas, which can inform on a specific ecosystem but will be more impacted by cloud cover, and large areas that might encompass different ecosystems or phytoplankton bloom dynamics but will undoubtedly have a higher number of valid satellite observations. In the latter case, several successive blooms might be the result of observations in different parts of the region at different times.

Finally, daily images were selected over 8-day composites as they provide the most convergences (i.e., greatest number of fits) and are most appropriate to capture the rapid changes in phytoplankton biomass during a bloom. Annex 1 (Figure A1 to Figure A4) shows annual times series at daily resolution and the corresponding fits.

Access to Data Products

Data products presented in the figures of this document are published on the Government of Canada’s Open website; a link to the data is available on request to the corresponding author. The daily chlorophyll-a concentration to estimate bloom metrics in each of the three regions presented in Figure 10 are available from the DFO Maritimes Region upon request. All the chemical data are available at Ocean Carbon Data System ([OCADS](#)).

RESULTS AND DISCUSSION

TOTAL INORGANIC CARBON AND PH

The Labrador Sea hosts a strong “solubility pump”—atmospheric anthropogenic CO₂ is sequestered to the deep ocean by chemical and physical processes. The depth of the Newly Ventilated Labrador Sea Water (NV-LSW) trapped by winter convection varies from year to year, ranging from 500 m to over 2,000 m. The average concentrations of TIC and pH, between

¹ Layton, C., Devred, E., and DeTracey, B. A comparison of phytoplankton spring bloom fitting methods using MODIS satellite-derived chlorophyll-a concentration for the Maritimes region. Can. Tech. Rep. Hydrogr. Ocean Sci. In Press.

150 and 500 m for stations located in the central part of the Labrador Basin, were used as representative concentrations for NV-LSW. TIC concentration increased by $18.52 \mu\text{mol kg}^{-1}$ from 1996 to 2018, reaching a maximum of $2,166.5 \mu\text{mol kg}^{-1}$ in 2018, in response to the local uptake of anthropogenic CO_2 (Figure 4). As a result, the pH decreased by 0.07 units during the same period (Figure 4) representing a decline rate of 0.003 y^{-1} . Trends between 1996 and 2018 were highly significant with a correlation coefficient, r^2 , explaining respectively 91% and 79% of the variance in TIC and pH. Arctic outflow and the local uptake of anthropogenic CO_2 in the deep-convection region of the Labrador Sea are major controlling mechanisms for the state of ocean acidification in the northwest Atlantic, and the continuous trend observed in our dataset could impact the entire northwest Atlantic. The Arctic water inflows to the highly productive regions in the northwest Atlantic, which have important commercial fisheries and make these regions more susceptible to future ocean acidification than other regions (Azetsu-Scott et al. 2010). Ocean acidification also influences the capacity of the ocean to take up CO_2 from the atmosphere.

TRANSIENT TRACERS CFC-12 AND SF₆

During the second half of the twentieth century, the atmospheric burden of CFCs increased steadily, due mainly to their widespread use as refrigerants and aerosol propellants. The invasive atmospheric flux of these mostly inert gases provided an excellent record of ocean circulation, and profiles of dissolved CFC-12 concentration have been measured annually along the AR7W line since 1991 (Figure 5). As a consequence of restrictions on the manufacture and use of ozone-depleting substances introduced in 1989, the atmospheric mixing ratio of CFC-12 has been in decline since 2003 and its capacity at tracking recent ventilation episodes has become limited (Figure 5). Measurements of an alternative transient tracer, SF₆, were introduced in 2011. There has been a rapid, near-linear increase in atmospheric SF₆ since 2011 and it is reflected in the dissolved concentration profiles of the recently ventilated water, represented by the layer of the Labrador Sea Central Basin between 150 and 500m (Figure 5), compared with CFC-12.

TEMPERATURE IN THE TOP 100 M

Temperatures recorded by the CTD sensor during the occupation were averaged between 0 and 100 m, which corresponds roughly to the temperature regime of the phyto- and mesozoo- plankton sampled layer. While the timing of the cruise affects the average temperature for a given region and year, removing the years 2003 and 2004 (due to later-than-usual sampling dates, Figure 2) from the reference period lowered it by about $0.2 \text{ }^\circ\text{C}$ and resulted in little effect on the anomaly patterns (not shown here). The Labrador Shelf (LS) exhibited a lower temperature (mean of approximately $1.1 \text{ }^\circ\text{C}$) than the Central Labrador Sea (CLS) (approximately $4.2 \text{ }^\circ\text{C}$) and the Greenland Shelf (GS) (mean of approximately $3 \text{ }^\circ\text{C}$) due to the inflow of Arctic water (Figure 6, top panels).

The CLS and GS warmest year occurred in 2003, while the warmest anomaly for the LS happened in 2009 (Figure 6, bottom panel). While temperatures on the CLS and GS have been continuously lower than average since 2013, the LS shows a succession of higher and lower values than normal (Figure 6). Labrador current flowing south is typically much colder than the CLS region and its eastern boundary moves longitudinally. The presence of ice is sometimes keeping us from sampling the shelf area, therefore returning a warmer-than-normal average temperature.

NUTRIENTS

All near-surface nutrient concentrations (i.e., 0–100 m, nitrate, phosphate, and silicate) exhibited inter-annual variations, between 1999 and 2013, with a generally increasing trend over time (Figure 7). In most cases, the variation in the anomalies of surface nutrient concentrations was consistent among the three regions of interest. Within a given region, concentrations among different nutrients were not always following the same trend, meaning that, for example, an above-average concentration of nitrate in a given year does not necessarily correspond to above-average concentrations for phosphate or silicate (see year 2008 on GS). Since 2014 anomalies, in all three regions, are steadily positive meaning the nutrient stocks in the surface have remained above average for that period. Deep nutrients (100+ m to bottom) showed a different pattern than the surface nutrients in agreement with the hydrodynamics of the Labrador Sea and the surface-layer biological activity (Figure 8). As expected, deep nutrients average concentrations were higher than surface nutrients concentrations because they were not consumed by phytoplankton and remineralization at depth replenishes the nutrient pool. Average concentrations from 100 m to 3000 m or less (depending on bathymetry) provide very rough estimates of the deep nutrient pool but do not inform on variations within and between water masses in the deep basin of the CLS. Deep nitrate on the GS and LS showed high inter-annual variability when compared to the CLS deep nitrate, which remained near the average concentration since 2010, with the exception of a drop in 2016. A similar pattern was also observed for the deep silicate in CLS, with an average concentration since 2011 (Hátún, H. et al. 2017). On the LS, nitrate and phosphate concentrations oscillated around the reference values, while average concentrations of silicate remained below normal since 2007. There were no emerging patterns in the inter-annual variability of nutrients from 2014 to 2018.

***IN SITU* CHLOROPHYLL-A CONCENTRATION**

In general, the Greenland Shelf region has high concentrations of chlorophyll-*a* (Figure 9) and is dominated by nanophytoplankton with low concentrations of picophytoplankton. Conversely, the Central Labrador Sea is a region with low chlorophyll-*a* concentrations and a low proportion of nanophytoplankton, with high concentrations of picophytoplankton. The Labrador Shelf region has the lowest concentrations of chlorophyll-*a* and nanophytoplankton, with intermediate concentrations of picophytoplankton. Upper ocean (< 100 m depth) phytoplankton sampled on the AR7W section in spring and early summer between 1999 and 2015 showed region-specific characteristics (Fragoso et al. 2016, Li and Harrison 2014).

Patterns of in situ chlorophyll-*a* concentration measured during the occupation of AR7W were generally consistent with observations of satellite-derived chlorophyll-*a* concentration, with low chlorophyll-*a* concentration on the Labrador Shelf and the Central Labrador Sea, and a relatively high chlorophyll-*a* concentration on the Greenland Shelf (Figure 9). This is explained by the input of nutrients and stratification resulting from the outflow of glacier melts that provide favorable conditions for phytoplankton growth. In the early 2000's (1999–2007), chlorophyll-*a* concentrations were generally lower than the average for the reference period for all three regions (Figure 9), which can partly be explained by the spring blooms occurring earlier than the cruise dates (Figures 2 and 10). From 2008 to 2014, chlorophyll-*a* concentrations were higher than the average for the reference period, again in all three regions.

Since 2014 chlorophyll-*a* concentrations have been lower than normal for all three regions, except for the Central Labrador Sea in 2015, when concentrations were above normal. These high concentrations were associated with an intense phytoplankton bloom dominated by *Phaeocystis* sp., which was observed directly from samples taken from the ship and analyzed by light microscopy, the bloom leading to clogging of zooplankton nets.

SATELLITE-DERIVED SPRING BLOOM INDICES

In general, the four metrics that describe the spring bloom were highly variable from year-to-year and among regions, so that no clear trends emerged (Figure 10). This is consistent with the ephemeral nature of phytoplankton blooms that respond in a rapid manner to favorable conditions of the chemical and physical environments. However, the results of satellite observations were also impacted by cloud cover which lead to data gaps, such that bloom peaks might have been missed in a given year and region. There was no statistical evidence of correlation among the metrics, so that, for example, an early bloom does not necessarily translate to a longer duration or higher amplitude. For instance, a later-than-average initiation on the LS in 2003 and 2018 had a longer duration than normal in 2018 but shorter duration than normal in 2003.

On average, the annual phytoplankton spring bloom started earlier on the Greenland Shelf (day of the year [doy] 123), than in the Central Labrador Sea (doy 126) and Labrador Shelf (doy 136) (Figure 10). From 2003 to 2013, there were no trends in the bloom metrics and each region shows its own pattern. Magnitude and amplitude of the bloom were higher on the Greenland Shelf than on the Labrador Shelf and Central Labrador Sea (Figure 10). This result was expected as this region is subject to freshwater inputs from the adjacent glacier, which increases stratification and the supply of nutrients (Gillard et al. 2016, Luo et al. 2016), and creates favorable conditions for phytoplankton blooms and sustained high primary production. An exceptional event occurred during the spring of 2015, when the timing of the bloom was particularly early in the Central Labrador Sea (starting mid-April, the earliest onset recorded since 2003), associated with the highest magnitude on record. Furthermore, these satellite observations were consistent with *in situ* measurements of chlorophyll-*a* concentration. (See section 5.4.) The Greenland Shelf bloom characteristics followed the same pattern as the Central Labrador Sea, while the Labrador Shelf bloom initiation and duration were about average, and the bloom amplitude and magnitude were higher than normal (Figure 10). Since 2016, bloom initiation dates have been delayed compared to the reference period averages for the Central Labrador Sea and Greenland Shelf and bloom magnitudes have shown no obvious patterns. The bloom magnitude in the Central Labrador Sea however has been consistently above average.

MESOOZOPLANKTON

Calanus finmarchicus copepods dominate the mesozooplankton biomass in the Central Labrador Sea, while it and its congeners *C. glacialis* and *C. hyperboreus* contribute about one third each on the shelves (Head et al. 2003). *C. finmarchicus* total abundances are greatly influenced by the abundance of young stage copepodites. These develop from eggs laid by females that have overwintered as pre-adults in the deep central basin and re-ascended in spring. The spring bloom provides the food to fuel egg-laying and subsequent population development, so that regional differences in spring bloom dynamics also lead to differences in the timing of the development of *C. finmarchicus* populations. Since spring blooms are generally earlier and more intense on the GS than elsewhere, *C. finmarchicus* populations are generally more abundant there than elsewhere at the time of in situ sampling (Figure 11).

On the Labrador Shelf, during the 1995 to 2018 period, there were two years with exceptionally high abundances for *C. finmarchicus*—1999 (June) and 2011 (May)—the reasons for which are unknown (Figure 11). Otherwise, abundances have been variable, with two higher-than-average values (June 2001 and July 2002) and a sustained period of relatively-low abundance between 2004 and 2008. Since 2013, abundances have been slightly below average.

In the Central Labrador Sea, because the spring bloom and the relatively late development of *C. finmarchicus*, *in situ* sampling in summer generally gave higher abundances than in spring, as indicated by the positive anomalies in 1995, 1999, 2002, and 2003 (Figure 11). Young stages were seldom very abundant, perhaps due to high mortality (Head et al. 2015), except for the summer of 1995, with an exceptionally higher total abundance year. There was no trend in springtime total abundance for *C. finmarchicus* between 1996 and 2014. Since 2015, however, abundances have been unusually low, perhaps owing to earlier sampling than in previous years (Figures 2 and 11).

On the Greenland Shelf, there was one exceptionally high *C. finmarchicus* abundance value in May 2006, the cause of which is unclear. Otherwise, higher-than-average values tended to be associated with later sampling dates (e.g., 1995, 1999, 2001–2003, and 2012), while relatively low abundances were associated with early sampling dates since 2012.

High abundance of *C. glacialis* and *C. hyperboreus* on the shelves may result from the transport of individuals in the inflows, since neither species have a local overwintering source population. The abundances of both species have generally shown considerable year-to-year variability, but with sustained periods of low abundance for *C. glacialis* on both shelves since 2014, and sustained periods of high abundance for *C. hyperboreus* on the GS between 2009 and 2012 and of low abundance on the LS since 2014. *C. hyperboreus* abundance on the GS was also low in 2018 (Figure 11).

Clausocalanidae, mainly represented here by the genus *Pseudocalanidae* spp, were persistently more abundant than the average in the CLS over the last 10 years, whereas a general decreasing trend was observed on LS and GS since 2014 (Figure 12). Unlike *Pseudocalanidae*, *Oithonidae* were persistently less abundant in the Central Labrador Sea for more than 10 years, while the decrease in abundance on both shelves became more prevalent around 2014 (Figure 12). Since 2014, *Euphausiid* abundances have been consistently lower than average in all regions (Figure 13). Amphipods, mostly represented here by *Parathemisto libellula*, showed higher-than-average abundances in the Central Labrador Sea in 2018. Being a species associated with Arctic water masses, this phenomenon is consistent with the cooler-than-average temperatures in the Central Labrador Sea during that year (Figure 13).

CONTINUOUS PLANKTON RECORDER

As a reminder, the time-series results in this section ended in 2017, because handling of the samples is time consuming and data are only released with a year time lag.

Phytoplankton

PCI values represent the average chlorophyll-a standing stock during the reference period from 1960 to 2009 (Figure 14). In the sub-polar gyre, decadal-average PCI values shifted from low to high in all regions between the 1980s and 1990s, and these patterns have persisted to the present. In 2017, PCIs were highest in regions east of the Newfoundland Shelf and they were still relatively high farther west. The same value/abundance tendencies were observed for PCIs, diatoms, and dinoflagellates for the decades prior to the 2010s. Since then, diatom and dinoflagellate abundances have remained high in the deep-water region adjacent to the Newfoundland Shelf (NS) between 40°W and 45°W (40–45). Farther east and on the NS and Scotian Shelf (SS), diatom abundances decreased somewhat after 2009 and a similar pattern was seen for dinoflagellates, except that the decreases in abundance were more pronounced east of 40–45. The apparent inconsistency between the recent increases in PCI and decreases in diatom and dinoflagellate abundances on the SS are thought to be related to the inclusion of

small forms (e.g., nanoflagellates) that are increasing in abundance, while larger forms (diatoms, dinoflagellates) are decreasing.

Mesozooplankton

Since the 1990s, annual abundances for *Calanus* I–IV (mostly *Calanus finmarchicus*) and *C. finmarchicus* V–VI) have been above average for regions 40–45 and farther east, decreasing during the 2010 to 2016 period on the SS, but increasing again in 2017 (Figure 15). Annual abundances for *C. glacialis* were low in most regions, with highest values in the 1990s or 2000s, decreasing in all regions thereafter, especially on the Western Scotian Shelf (WSS) and excepting the 40–45 region, where abundances remained high (Figure 15). Average annual abundances for *C. hyperboreus* were high in all regions in 2017, which might be related to recent intense deep-water convection and increase in primary production in the Labrador and Irminger Seas.

In 2017, the annual average abundances of the three small copepod groups (Copepod nauplii, *Para/Pseudocalanus*, and *Oithona*) all showed positive anomalies within all regions, except on the SS, where *Para/Pseudocalanus* and *Oithona* were very low or close to average, respectively (Figure 16). In the sub-polar gyre, decadal annual anomalies for copepod nauplii and *Paracalanus/Pseudocalanus* have been higher since the 1990s than they were in previous decades. For the shelf regions, however, while the decadal annual abundance anomalies for copepod nauplii followed the same pattern, for *Para/Pseudocalanus* the opposite pattern was seen, with relatively higher anomalies until the 1990s and low abundances since 2017. Decadal annual abundances for *Oithona* spp. were generally close to average throughout all regions until the 2000s; thereafter they remained close to average in most regions, but were higher than average in the 40–45 region in 2010–2013 and on the NS in 2014.

Macrozooplankton

Average annual abundances for *Euphausiids* and *Hyperiid* amphipods were generally higher in the deep-ocean regions of the sub-polar gyre than over the shelves, and are highest in the 40–45 region (Figure 17). In the sub-polar gyre *Euphausiid* decadal abundance anomalies were generally close to average in the 1960s–1990s, but decreased in the 2000s, remaining low thereafter. In shelf regions, *Euphausiid* abundance anomalies have shown a downward trend since the 1970s. Abundance anomalies for *Hyperiid* amphipods have generally shown increasing trends in all regions since the 1960s, albeit with low values on the NS region in the 2000s and in the 25–30 region in the 2010–2016 period.

Acid sensitive taxa

Coccolithophores (phytoplankton) and foraminifera (microzooplankton) have only been counted systematically in CPR samples since 1991, while pteropods belonging to the genus *Limacina*, have been counted since the inception of the CPR Survey. Average annual abundances of coccolithophores and foraminifera (forams) increased in all regions in the 2010–2016 period and remained high in abundance in 2017, except in the case of coccolithophores on the SS, which decreased to below-average values in 2017 (Figure 18). The abundance of *Limacina* increased in the 1990s, compared with previous decades, and has generally remained at near-average or above-average values since.

SUMMARY

The Atlantic Zone Off-Shelf Monitoring Program (AZOMP) provides observations on ocean climate and plankton variability within the Labrador Sea and adjacent shelves affecting

ecosystems of Atlantic Canada and climate from a regional to global scale. In the Labrador Sea, surface heat losses in winter result in the formation of dense waters, which spread across the ocean, ventilating the deep layers, thus contributing to the global ocean-overturning circulation. Since 2014, the mid-high latitude North Atlantic experienced moderate to high surface heat loss leading to elevated convective mixing during the winter period, and significant formation of Labrador Sea Water (LSW), among the highest in terms of volume and depth.

Strong inter-annual variability was observed in surface nutrient concentrations, which are consistent among regions. Since 2014, there have been positive anomalies in all regions, with a trend that started in 2013 in the CLS for nitrate, phosphate, and silicate. The CLS showed an average nitrate concentration in 2015, however, likely breaking the trend of high anomalies, as a result of the nutrient draw down caused by the abnormally large bloom observed in that year. Chlorophyll-*a* concentrations have followed a similar pattern, with lower than normal concentrations for all three regions since 2014, except for the anomalously high concentration in 2015. These were associated with an intense phytoplankton bloom consisting mainly of *Phaeocystis* sp., which was identified from shipboard observations. Ocean color metrics of the phytoplankton spring bloom (initiation, duration, magnitude, and amplitude) showed no obvious trends over time, and each region revealed its own pattern. Satellite observations are impacted by cloud cover, resulting in data gaps that might miss the peak of the bloom in a given year and region. Recurrent earlier sampling dates from year to year may partly explain the observed downward trends in in-situ phytoplankton abundances, since sampling may have occurred before the start of the seasonal spring bloom.

The 0–100 m abundances of several mesozooplankton taxa followed a pattern similar to that shown by phytoplankton (chlorophyll-*a*) concentration, with lower-than-average abundances since 2014. For some taxa, this may be linked in part to their seasonal life-cycles, since earlier sampling in recent years means that the populations were less developed (i.e., include fewer members of the new year's generation). Interestingly, the unusually intense bloom of 2015 did not appear to have any effect on the abundances of any of the mesozooplankton taxa.

Finally, long-term observations of annual average abundances of phytoplankton by means of the CPR indicate that all phytoplankton forms have increased in abundance since the 1990s, although more recently, abundances of smaller forms have continued to increase, while those of larger forms have decreased. In the sub-polar gyre, the abundance of the ecologically significant copepod *Calanus finmarchicus* has been higher since the 1990s, as have the abundances of three small copepod taxa. Similarly, the abundance of *Hyperiid* amphipods increased in the sub-polar gyre after the 1990s but, in contrast, the abundance of *Euphausiids* decreased. None of the three acid-sensitive taxa appear to have been affected by recent decreases in pH, given, as yet, the changes are small.

ACKNOWLEDGEMENTS

The authors thank the sea-going staff of the Bedford Institute of Oceanography and the officers and crew of the Canadian Coast Guard ships Hudson. Jay Barthelotte, Robert Benjamin, Jay Bugden, Diana Cardoso, Carla Caverhill, Terry Cormier, Jennifer Field, Adam Hartling, Flo Hum, Jeff Jackson, Matt Lawson, Dave Levy, Kevin MacIsaac, Cathy Porter, Tim Perry, Peter Thamer, Richard Nelson, Melissa Falkner, and Darlene Childs contributed to sample collection, sample analysis, data analysis, data management, and data sharing. Thanks to reviewers David Bélanger and David Brickman whose comments really improved the manuscript.

REFERENCES CITED

- Astthorsson, O.S., and Gislason, A. 2003. [Seasonal variations in abundance, development and vertical distribution of *Calanus finmarchicus*, *C. hyperboreus* and *C. glacialis* in the East Icelandic Current](#). Journal of Plankton Research 25(7): 843–854.
- Azetsu-Scott, K., Clarke, A., Falkner, K., Hamilton, J., Jones, E.P., Lee, C., Petrie, B., Prinsenber, S., Starr, M., and Yeats, P. 2010. [Calcium Carbonate Saturation States in the waters of the Canadian Arctic Archipelago and the Labrador Sea](#). Journal of Geophysical Research 115: C11021.
- Becker, S., Aoyama, M., Woodward, E.M.S., Bakker, K., Coverly, S., Mahaffey, C., and Tanhua, T. 2019. [GO-SHIP Repeat Hydrography Nutrient Manual: The precise and accurate determination of dissolved inorganic nutrients in seawater, using Continuous Flow Analysis methods](#). In: [The GO-SHIP Repeat Hydrography Manual: A Collection of Expert Reports and Guidelines](#).
- Caldeira, K. and Wickett, M.E. 2003. [Anthropogenic carbon and ocean pH](#). Nature.425: 365
- Denman, K. L. and Platt, T. 1975. Coherences in the horizontal distributions of phytoplankton and temperature in the upper ocean. Mem. Soc. r. Sci. Liège 6e série 7: 19–30.
- Dickson, A.G., Sabine, C.L., and Christian, J.R. (Eds.) 2007. [Guide to Best Practices for Ocean CO₂ Measurements](#). PICES Special Publication 3. 191 pp.
- Feely, R.A., Sabine, C.L., Lee, K., Berelson, W., Kleypas, J., Fabry, V.J., and Millero, F.J. 2004. [Impact of Anthropogenic CO₂ on the CaCO₃ System in the Oceans](#). Science. 305(5682): 362–366.
- Fragoso, G.M., Poulton, A.J., Yashayaev, I.M., Head, E.J.H., Stinchcombe, M.C., and Purdie, D.A. 2016. [Biogeographical patterns and environmental controls of phytoplankton communities from contrasting hydrographical zones of the Labrador Sea](#). Progress in Oceanography 141: 212–226.
- Gillard, L. C., Hu, X., Myers, P. G., and Bamber, J. L. 2016. [Meltwater pathways from marine terminating glaciers of the Greenland ice sheet](#). Geophysical Research Letters. 43:10,873-10,882.
- Haine, T. W. N. and Hall, T.M. 2002. [A generalized transport theory: Water mass composition and age](#). Journal Physical Oceanography. 32:1932–1946.
- Hall, T. M., Haine, T. W. N., and Waugh, D. W. 2002. [Inferring the concentration of anthropogenic carbon in the ocean from tracers](#). Global Biogeochemical Cycles. 16(4):1131. doi:10.1029/2001GB001835
- Harrison, W.G. and Li, W.K.W. 2008. [Phytoplankton growth and regulation in the Labrador Sea: light and nutrient limitation](#). J. Northwest. Atl. Fish. 39:71–82.
- Hátún, H., Azetsu-Scott, K., Somavilla, R., Rey, F., Johnson, C., Mathis, M., Mikolajewicz, U., Coupel, P., Tremblay, J.-É., Hartman, S., Pacariz, S.V., Salter, I., and Ólafsson, J. 2017. [The subpolar gyre regulates silicate concentrations in the North Atlantic](#). Scientific Reports 7(1): 14576.
- Head, E.J.H., Harris, L.R., and Yashayaev, I. 2003. [Distributions of *Calanus* spp. and other mesozooplankton in the Labrador Sea in relation to hydrography in spring and summer \(1995–2000\)](#). Progress in Oceanography 59(1): 1–30.

-
- Head, E.J.H., Gentleman, W.C., and Ringuette, M. 2015. [Variability of mortality rates for *Calanus finmarchicus* early life stages in the Labrador Sea and the significance of egg viability](#). *Journal of Plankton Research* 37(6): 1149–1165.
- Holm-Hansen, O., Lorenzen, C.J., Holmes, R.W., and Strickland, J.D.H. 1965. [Fluorometric Determination of Chlorophyll](#). *ICES Journal of Marine Science* 30(1): 3–15.
- Hood, E.M., Sabine, C.L. and Sloyan, B.M. (eds) 2010. [The GO-SHIP Repeat Hydrography Manual: a collection of expert reports and guidelines, Version 1](#). (IOCCP Report 14), (ICPO Publication Series 134).
- Johnson, K.M., Sieburth, J.M., Williams, P.J. leB, and Brändström, L. 1987. [Coulometric total carbon dioxide analysis for marine studies: Automation and calibration](#). *Marine Chemistry* 21(2): 117–133.
- Jones, P.D. and Hulme, M. 1996. [Calculating regional climatic time series for temperature and precipitation: methods and illustrations](#). *International Journal of Climatology* 16(4): 361–377. John Wiley & Sons, Ltd.
- Kérouel, R. and Aminot, A. 1997. [Fluorometric determination of ammonia in sea and estuarine waters by direct segmented flow analysis](#). *Marine Chemistry* 57(3): 265–275.
- Li, W.K.W. and Harisson, W.G. 2014. [The state of phytoplankton and bacterioplankton in the Labrador Sea: Atlantic Zone Off-Shelf Monitoring Program 1994–2013](#). *Can. Tech. Rep. Hydrogr. Ocean. Sci.* 302:xviii+181p.
- Lozier, M. S., Li, F., Bacon, S., Bahr, F., Bower, A.S., Cunningham, S.A., De Jong, M.F., De Steur, L., DeYoung, B., Fischer, J., Gary, S.F., Greenan, B.J.W., Holliday, N.P., Houk, A., Houpert, L., Inall, M.E., Johns, W.E., Johnson, H.L., Johnson, C., Karstensen, J., Koman, G., Le Bras, I.A., Lin, X., MacKay, N., Marshall, D.P., Mercier, H., Oltmanns, M., Pickart, R.S., Ramsey, A.L., Rayner, D., Straneo, F., Thierry, V., Torres, D.J., Williams, R.G., Wilson, C., Yang, J., Yashayaev, I., and Zhao, J. 2019. [A sea change in our view of overturning in the subpolar North Atlantic](#). *Science* 363(6426): 516.
- Luo, H., Castelao, R.M., Rennermalm, A.K., Tedesco, M., Bracco, A., Yager, P.L., and Mote, T.L. 2016. [Oceanic transport of surface meltwater from the southern Greenland ice sheet](#). *Nature Geoscience* 9(7): 528–532.
- Mitchell, M.R., Harrison, G., Pauley, K., Gagné, A., Maillet, G., and Stain, P. 2002. [Atlantic zonal monitoring program sampling protocol](#). *Can. Tech. Rep. Hydrogr. Ocean Sci.* 223: iv + 23p.
- Neill, C., Johnson, K.M., Lewis, E., and Wallace, D.W.R. 1997. [Accurate headspace analysis of *f*CO₂ in discrete water samples using batch equilibration](#). *Limnology and Oceanography* 42(8): 1774–1783.
- Platt, T. and Jassby, A.D. (1976), [The relationship between photosynthesis and light for natural assemblages of coastal marine phytoplankton](#). *Journal of Phycology* 12: 421–430.
- Richardson, A.J., Walne, A.W., John, A.W.G., Jonas, T.D., Lindley, J.A., Sims, D.W., Stevens, D., and Witt, M. 2006. [Using continuous plankton recorder data](#). *Progress in Oceanography* 68(1): 27–74.
- Sabine, C.L., Feely, R.A., Gruber, N., Key, R.M., Lee, K., Bullister, J.L., Wanninkhof, R., Wong, C.S., Wallace, D.W.R., Tilbrook, B., Millero, F.J., Peng, T.-H., Kozyr, A., Ono, T., and Rios, A.F. 2004. [The Oceanic Sink for Anthropogenic CO₂](#). *Science* 305(5682): 367.
-

-
- Wang, Z., Brickman, D., Greenan, B.J.W., and Yashayaev, I. 2016. [An abrupt shift in the Labrador Current System in relation to winter NAO events](#). *Journal of Geophysical Research: Oceans* 121(7): 5338–5349.
- Welschmeyer, N.A. 1994. [Fluorometric analysis of chlorophyll a in the presence of chlorophyll b and pheopigments](#). *Limnology and Oceanography* 39(8): 1985–1992.
- Yashayaev, I. and Loder, J.W. 2017. [Further intensification of deep convection in the Labrador Sea in 2016](#). *Geophysical Research Letters* 44(3): 1429–1438.
- Yashayaev, I., Peterson I., and Wang Z. 2021. [Meteorological, Sea Ice and Physical Oceanographic Conditions in the Labrador Sea during 2018](#). DFO Can. Sci. Advis. Sec. Res. Doc. 2021/042. v + 26 p.
- Yebra, L., Harris, R.P., Head, E.J.H., Yashayaev, I., Harris, L.R., and Hirst, A.G. 2009. [Mesoscale physical variability affects zooplankton production in the Labrador Sea](#). *Deep Sea Research Part I: Oceanographic Research Papers* 56(5): 703–715.
- Yentsch, C. and Menzel, D. 1963. [A Method for the Determination of Phytoplankton Chlorophyll and Phaeophytin by Fluorescence](#). *Deep-Sea Research* 10(3): 221–231.
- Zhai, L., Platt, T., Tang, C., Sathyendranath, S., and Walls, R.H. 2011. [Phytoplankton phenology on the Scotian Shelf](#). *ICES J. Mar. Sci.* 68(4): 781–791.

TABLES

Table 1. Atlantic Zone Off-Shelf Monitoring Program sampling missions between 2014 and 2018.

Year	Mission ID	Dates	Number of Hydro Stations	Number of BIO Stations	Number of Net Stations
2014	HUD2014-007	6–15 May	32	7	27
2015	HUD2015-006	6–18 May	30	7	29
2016	HUD2016-006	5–15 May	24	7	27
2017	No mission	-	-	-	-
2018	HUD2018-008	3–9 May	23	7	22

FIGURES

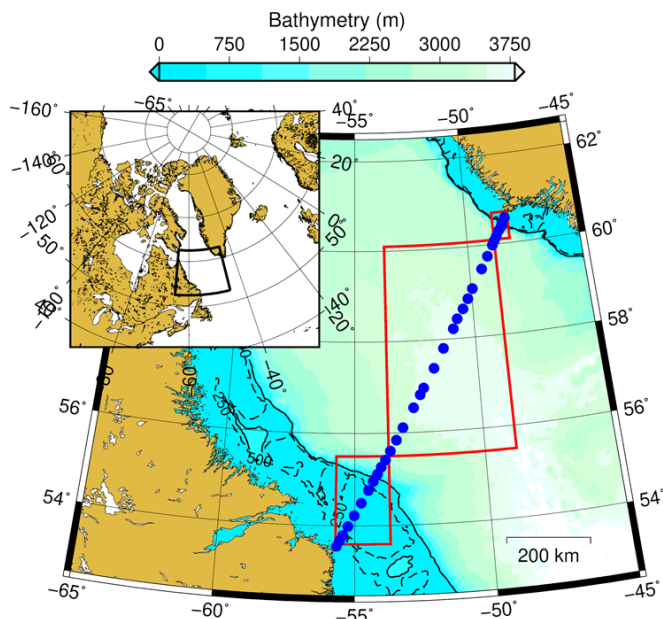


Figure 1. AR7W transect within the Labrador Sea. Blue dots represent the location of the core stations. Red boxes correspond to the regions where satellite chlorophyll-a concentration is extracted (i.e., Labrador Shelf, Central Labrador Sea and Greenland Shelf). Solid and dashed black lines correspond to the 500 and 250 m isobaths, respectively.

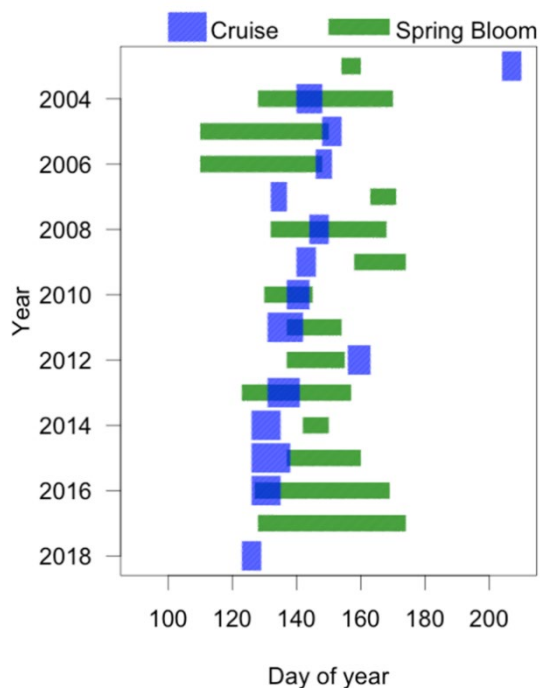


Figure 2. Bloom metrics for the Central Labrador Sea. Blue rectangles represent the sampling period (actual occupation of AR7W line) and green rectangles correspond to the duration of the spring bloom in the Central Labrador Sea as derived by satellite ocean colour. All dates are in Julian days. Vessel availability lead to the absence of a mission in 2017 and the heavy cloud cover in 2018 prevented a reliable description of the phytoplankton bloom.

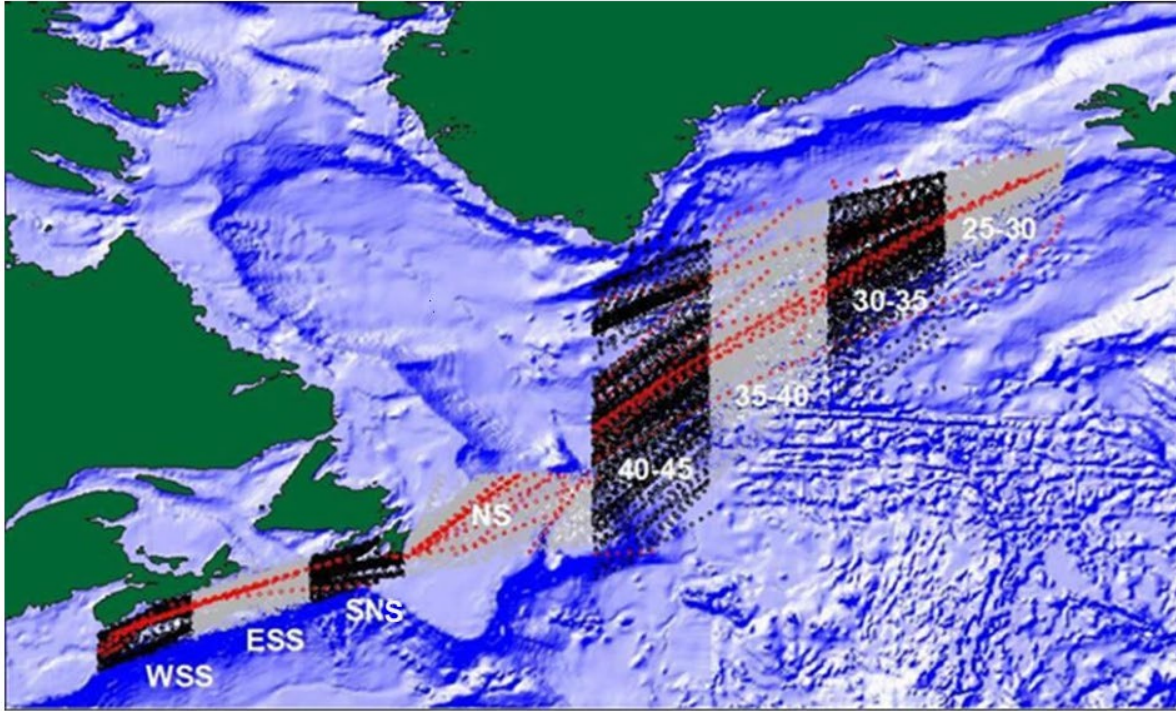


Figure 3. Continuous Plankton recorder (CPR) lines and stations 1957 to 2017. Stations sampled in 2017 are shown in red. Data are analyzed by region. Regions are: Western Scotian Shelf (WSS), Eastern Scotian Shelf (ESS), South Newfoundland Shelf (SNS), Newfoundland Shelf (NS), and between longitudes 40–45°W, 35–40°W, 30–35°W, 25–30°W.

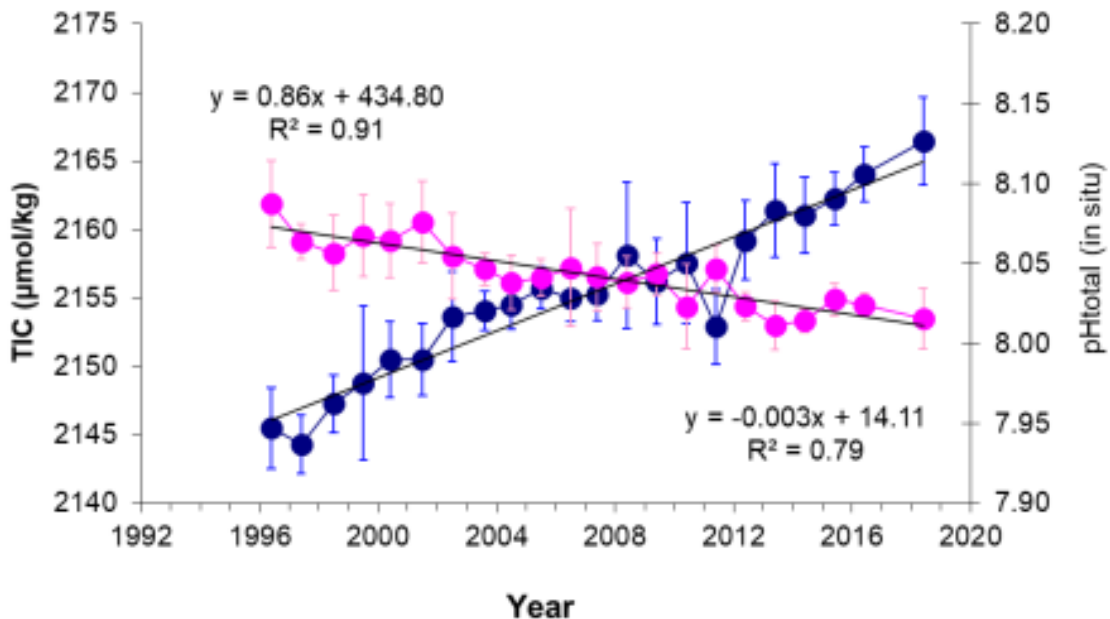


Figure 4. Time series of Total Inorganic Carbon (TIC; blue solid circles) and pH (pink solid circles) within the Newly-Ventilated Labrador Sea Water defined as 150–500 m in the Central Labrador Sea (CLS). Vertical bars indicate one standard deviation and black solid lines correspond to the linear regression of TIC and pH against time in year for stations located in the CLS for the period 1996–2018.

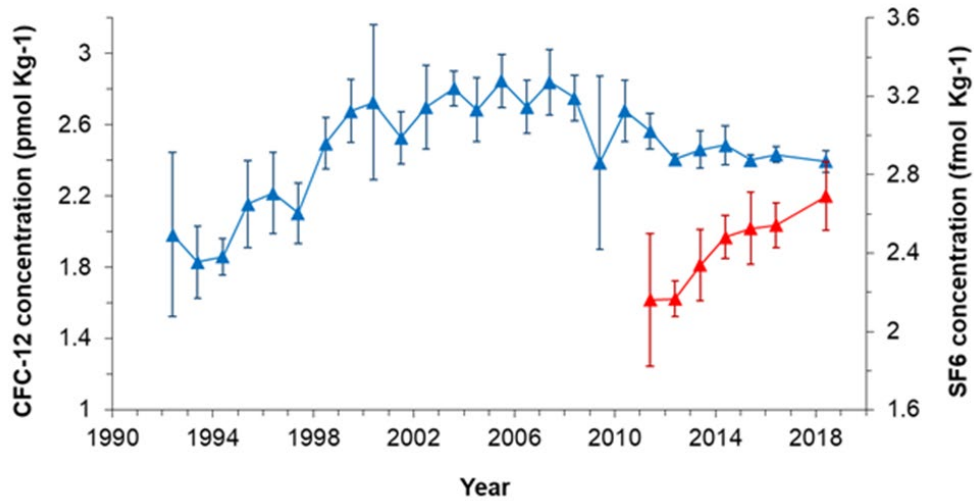


Figure 5. Annual mean concentrations of CFC-12 (blue solid triangles) and SF₆ (red solid triangles) in Newly-Ventilated Labrador Sea Water defined as 150–500 m in the Central Labrador Sea from 1991 to 2018. Vertical bars indicate one standard deviation.

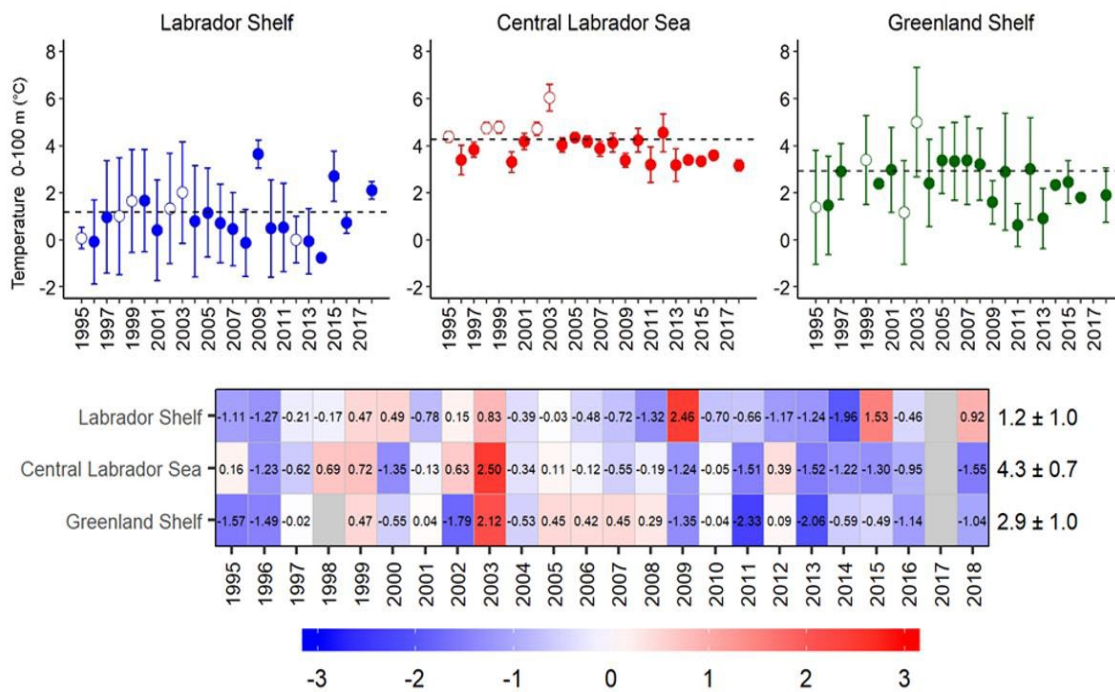


Figure 6. Top three panels: Mean annual surface temperature (in °C) measured from downcast Conductivity, Temperature, Depth (CTD) from the surface to 100 m for the Labrador Shelf (blue), Central Labrador Sea (red,) and Greenland Shelf (green). Open circles correspond to years with later-than-normal sampling (i.e., end of June/early July). The dashed lines indicate the average value of the reference period (1999–2010) and vertical bars indicate one standard deviation. The bottom panel shows the same data expressed in normalized anomalies (dimensionless) based on the same reference period. Numbers in the scorecards' cells represent the annual standardized anomalies. Numbers on the right side indicate the mean values 1999–2010 (i.e., reference) for a given region as well as the standard deviation (i.e., mean ± standard deviation).

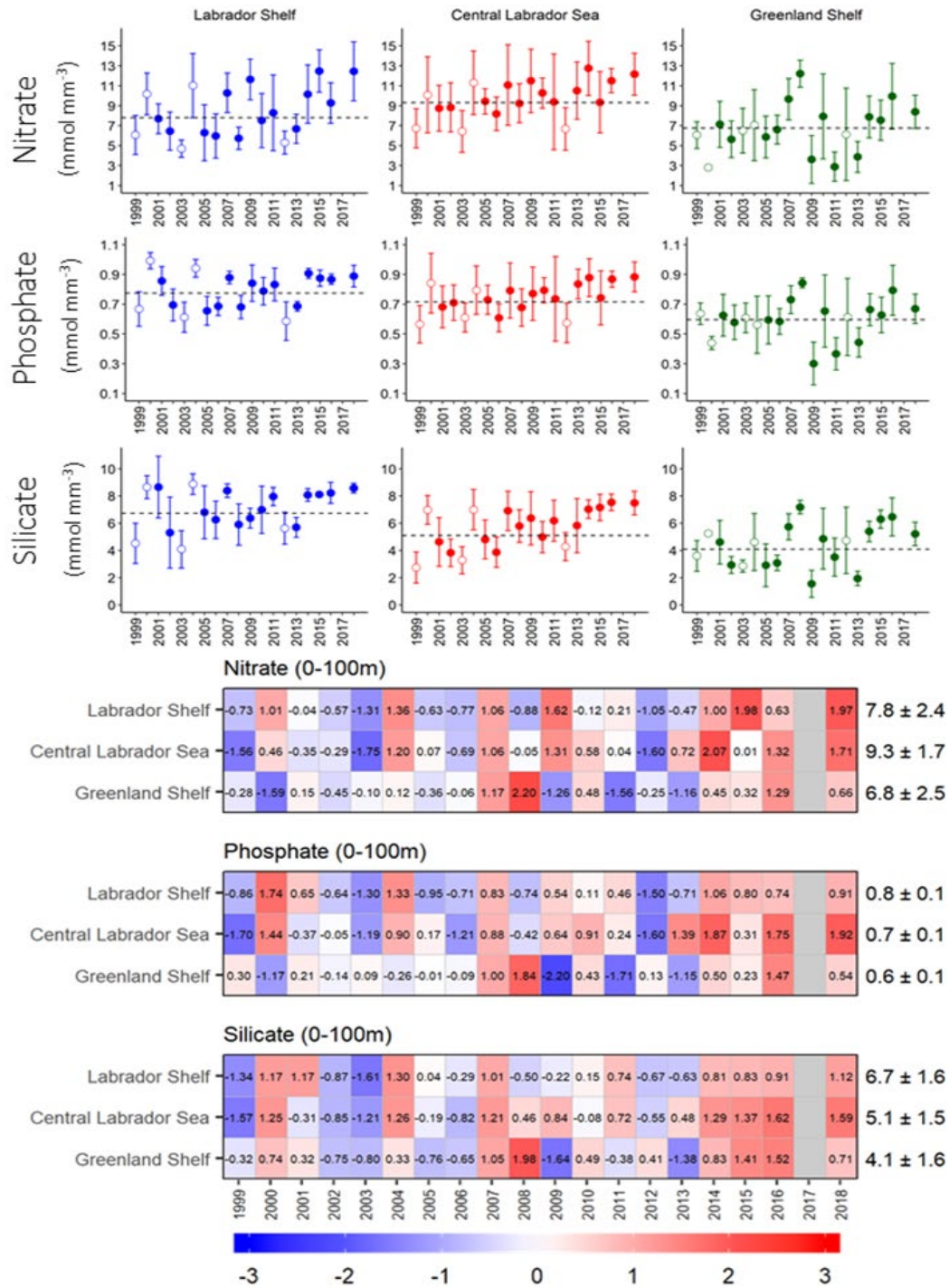


Figure 7. Top panels: Mean annual averaged surface (< 100 m depth) nutrient concentrations for the Labrador Shelf (blue), Central Labrador Sea (red), and Greenland Shelf (green). Open circles correspond to years with later-than-normal sampling (i.e., end of June/early July). The dashed lines indicate the average value of the reference period (1999–2010) and vertical bars indicate one standard deviation. Bottom panels: Scorecards for surface nutrients from 1999 to 2018 for the LS, CLS, and GS. Grey boxes indicate no data. Numbers in the scorecards' cells represent the annual standardized anomalies. Numbers on the right side indicate the mean values 1999–2010 (i.e., reference) for a given region as well as the standard deviation (i.e., mean ± standard deviation).

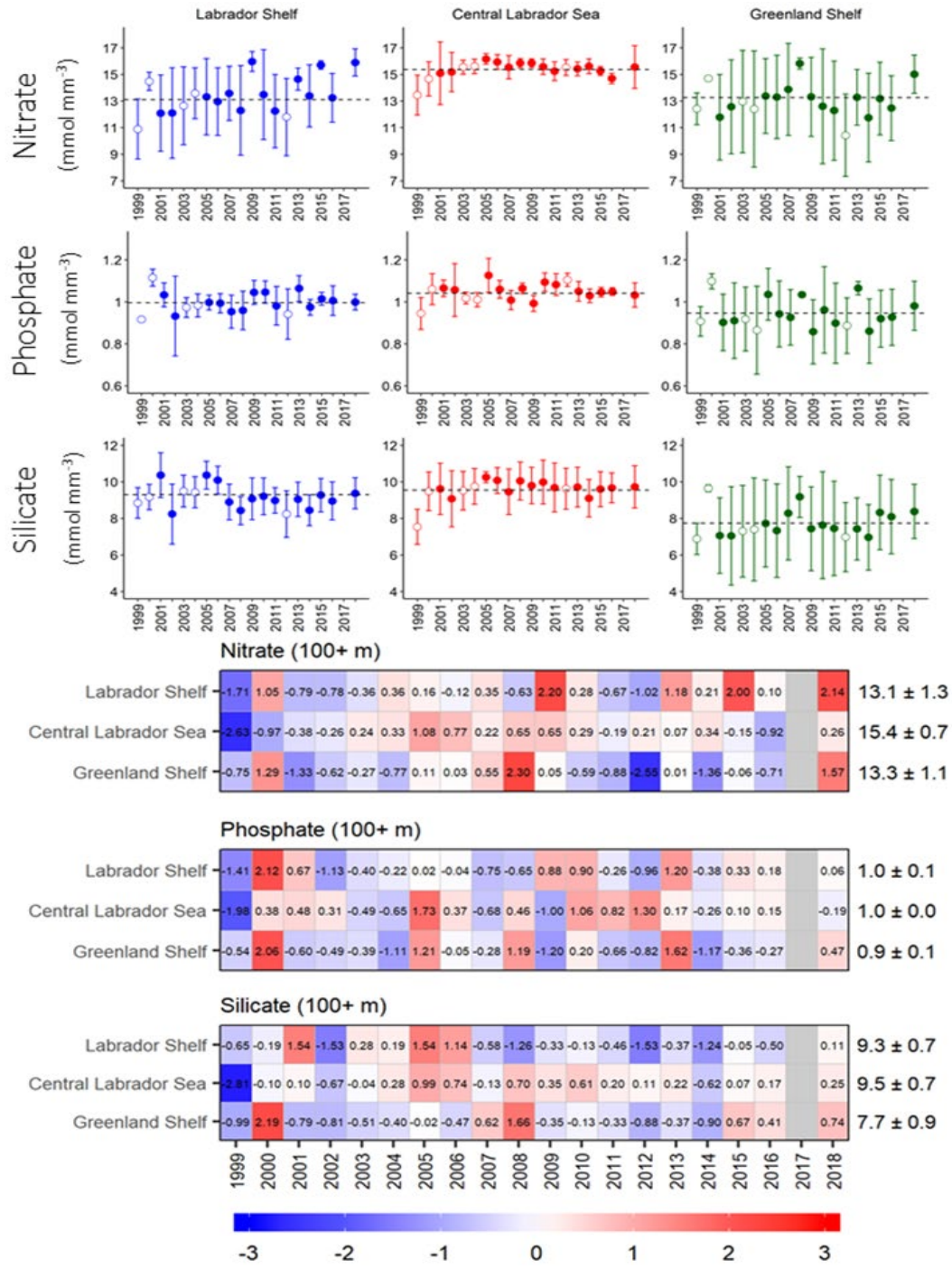


Figure 8. Top panels: Mean annual-averaged deep (100+ m) nutrient concentrations for the Labrador Shelf (blue), Central Labrador Sea (red), and Greenland Shelf (green). Open circles correspond to years with later-than-normal sampling (i.e., end of June/early July). The dashed lines indicate the average value of the reference period (1999–2010) and vertical bars indicate one standard deviation. Bottom panels: Scorecards for deep nutrients from 1999 to 2018 for the LS, CLS, and GS. Grey boxes indicate no data. Numbers in the scorecards' cells represent the annual standardized anomalies. Numbers on the right side indicate the mean values 1999–2010 (i.e., reference) for a given region as well as the standard deviation (i.e., mean ± standard deviation).

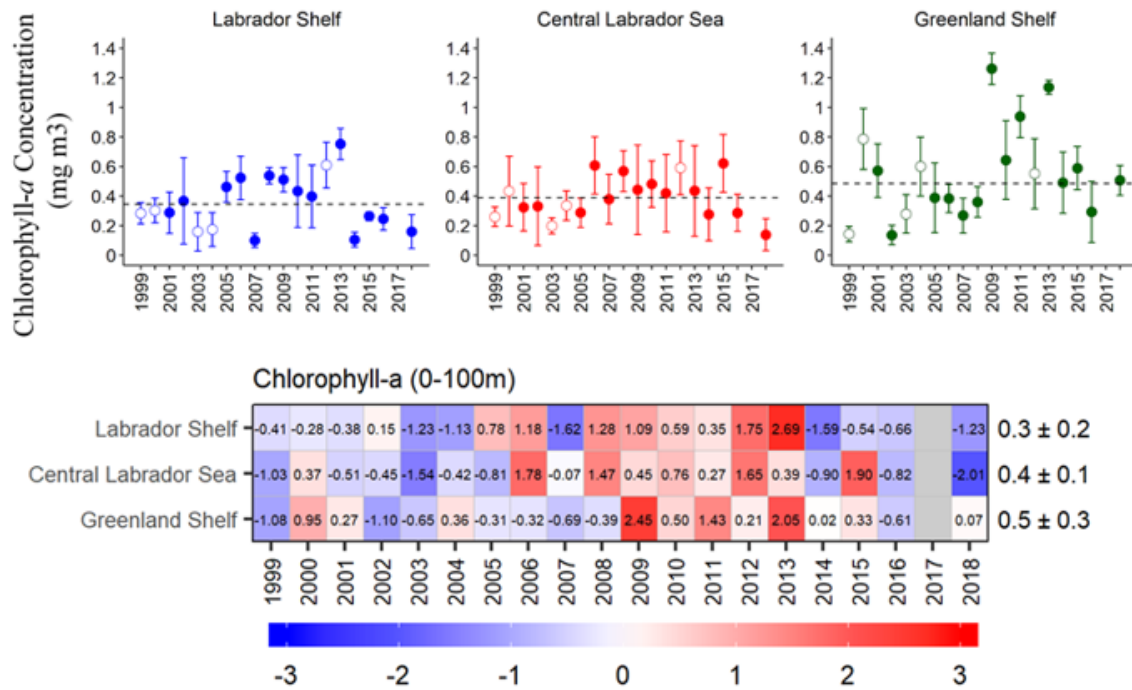


Figure 9. Top three panels: Mean annual averaged surface (< 100 m depth) chlorophyll-a concentrations for the Labrador Shelf (blue), Central Labrador Sea (red), and Greenland Shelf (green). Open circles correspond to years with later-than-normal sampling (i.e., end of June/early July). The dashed lines indicate the average value of the reference period (1999–2010) and vertical bars indicate one standard deviation. Bottom panel: Scorecards from 1999 to 2018 for the LS, CLS, and GS. Grey boxes indicate no data. Numbers within cells represent the annual standardized anomalies. Numbers on the right side indicate the mean values 1999–2010 (i.e., reference period) for a given region as well as the standard deviation (i.e., mean \pm standard deviation).

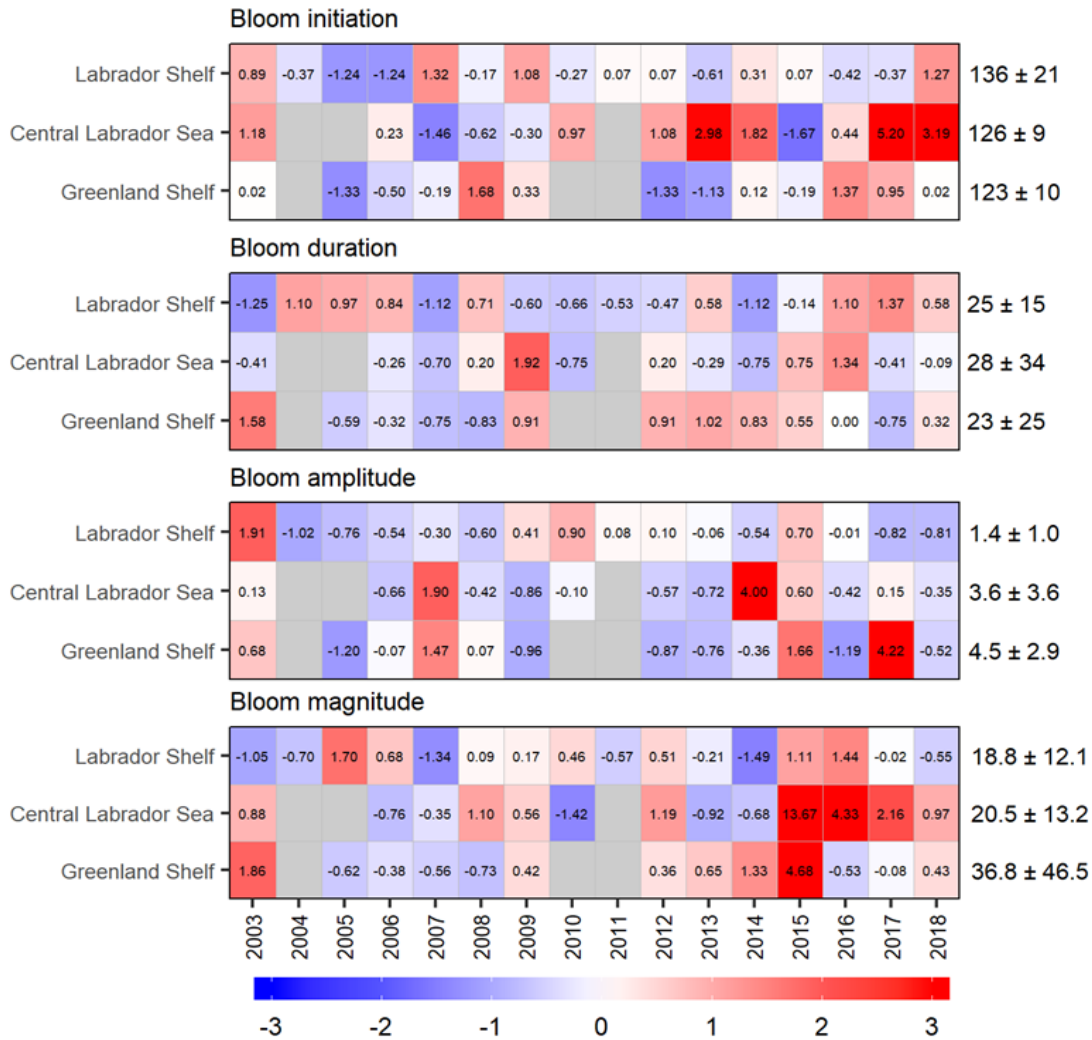


Figure 10. Scorecards for the bloom metrics (dimensionless) from 2003 to 2018 for the Labrador Shelf, Central Labrador Sea, and Greenland Shelf. Grey boxes indicate no data. Numbers within cells represent the annual standardized anomalies. Numbers on the right side indicate the mean values 1999–2010 (i.e., reference period) for a given region as well as the standard deviation (i.e., mean ± standard deviation).

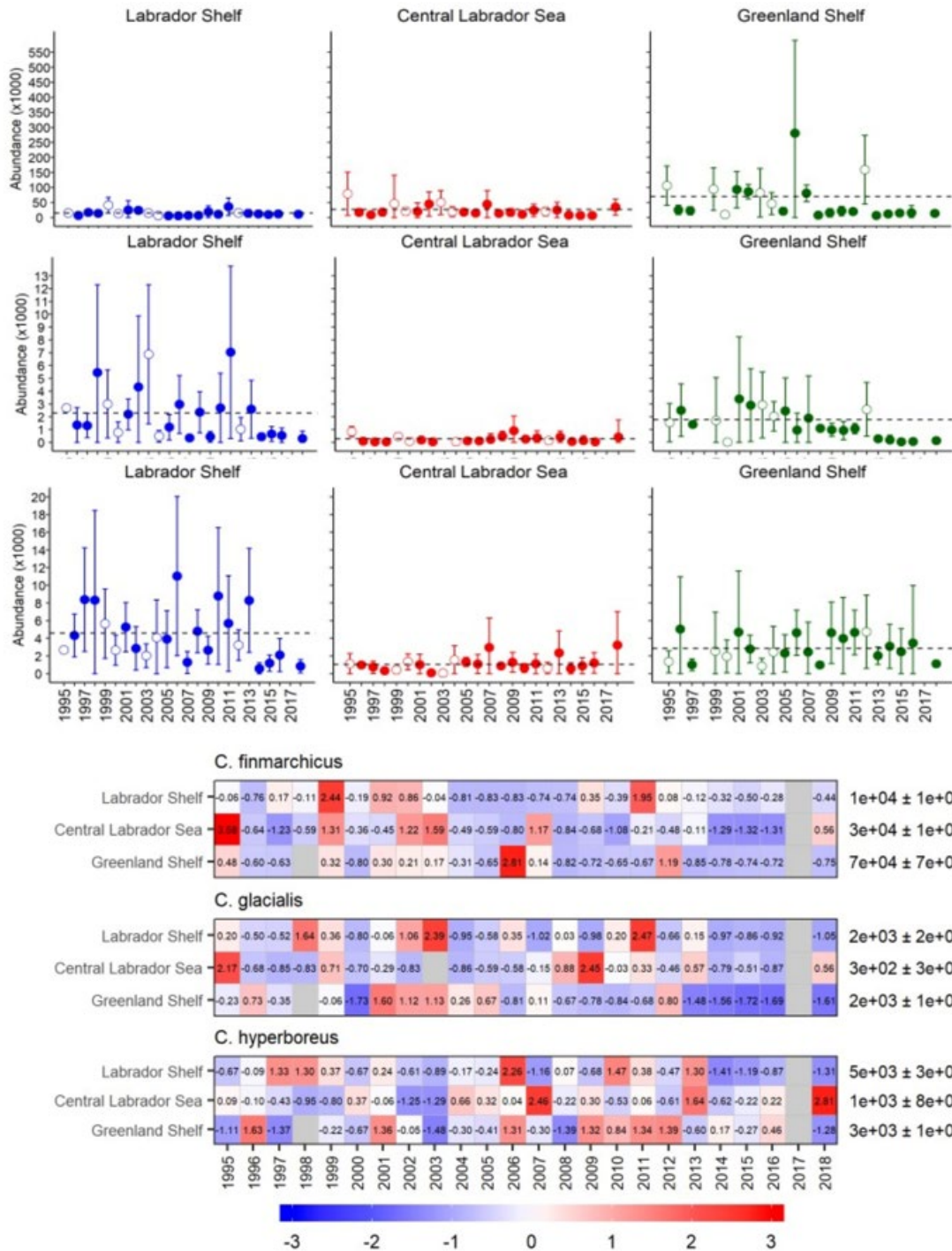


Figure 11. *Calanus finmarchicus*, *C. glacialis*, and *C. hyperboreus* abundances from 1995 to 2018 for the Labrador Shelf (blue), Central Labrador Sea (red), and Greenland Shelf (green). Open circles correspond to years with later-than-normal sampling (i.e., end of June/early July). The dashed lines indicate the average value of the reference period (1999–2010) and vertical bars indicate one standard deviation. The bottom panel shows the same data expressed in normalized anomalies (dimensionless) based on the same reference period. Grey boxes indicate no data. Numbers within cells represent the annual standardized anomalies. Numbers on the right side indicate the mean values 1999–2010 (i.e., reference period) for a given region as well as the standard deviation (i.e., mean ± standard deviation).

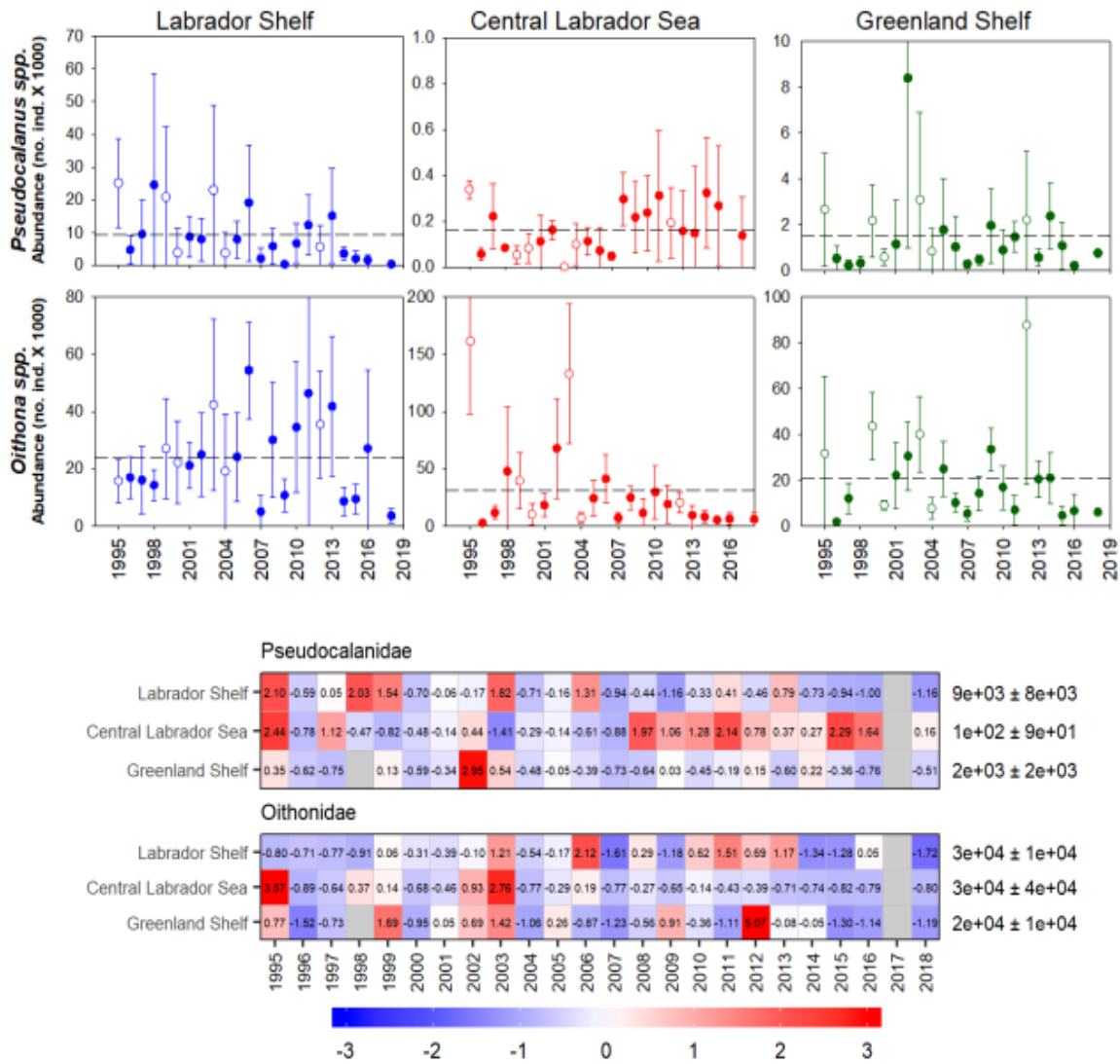


Figure 12. *Pseudocalanus* spp. and *Oithona* spp. anomalies of abundances from 1995 to 2018 for the Labrador Shelf (blue), Central Labrador Sea (red) and Greenland Shelf (green). Open circles correspond to years with later-than-normal sampling (i.e., end of June/early July). The dashed lines indicate the average value of the reference period (1999–2010) and vertical bars indicate one standard deviation. The bottom panel shows the same data expressed in normalized anomalies (dimensionless) based on the same reference period. Grey boxes indicate no data. Numbers on the right side indicate the mean values 1999–2010 (i.e., reference period) for a given region as well as the standard deviation (i.e., mean ± standard deviation).

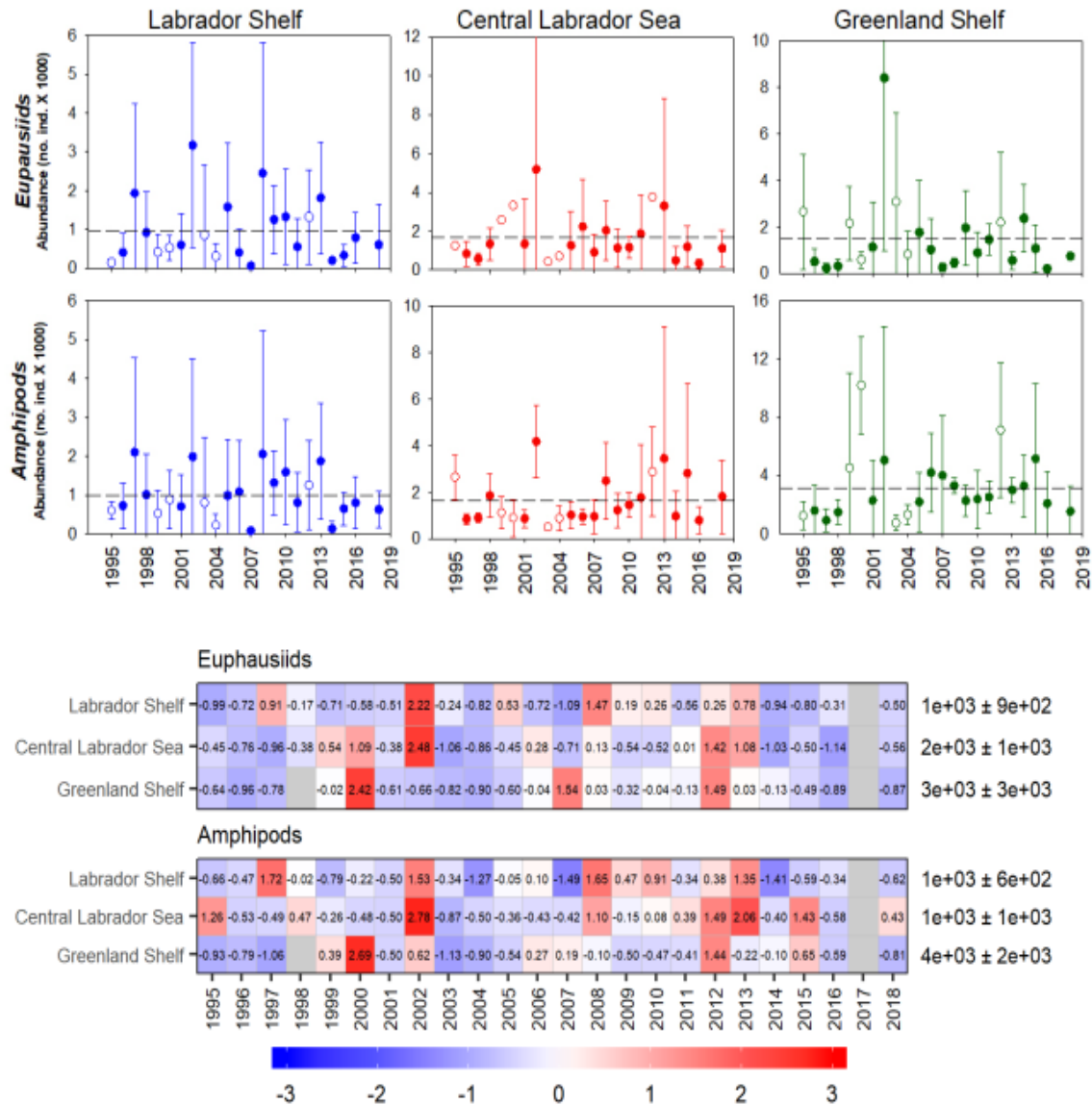


Figure 13. Euphausiid and Hyperiid (Amphipode) anomalies of abundances from 1995 to 2018 for the Labrador Shelf (blue), Central Labrador Sea (red), and Greenland Shelf (green). Open circles correspond to years with later-than-normal sampling (i.e., end of June/early July). The dashed lines indicate the average value of the reference period (1999–2010) and vertical bars indicate one standard deviation. The bottom panel shows the same data expressed in normalized anomalies (dimensionless) based on the same reference period. Grey boxes indicate no data. Numbers on the right side indicate the mean values 1999–2010 (i.e., reference period) for a given region as well as the standard deviation (i.e., mean \pm standard deviation).

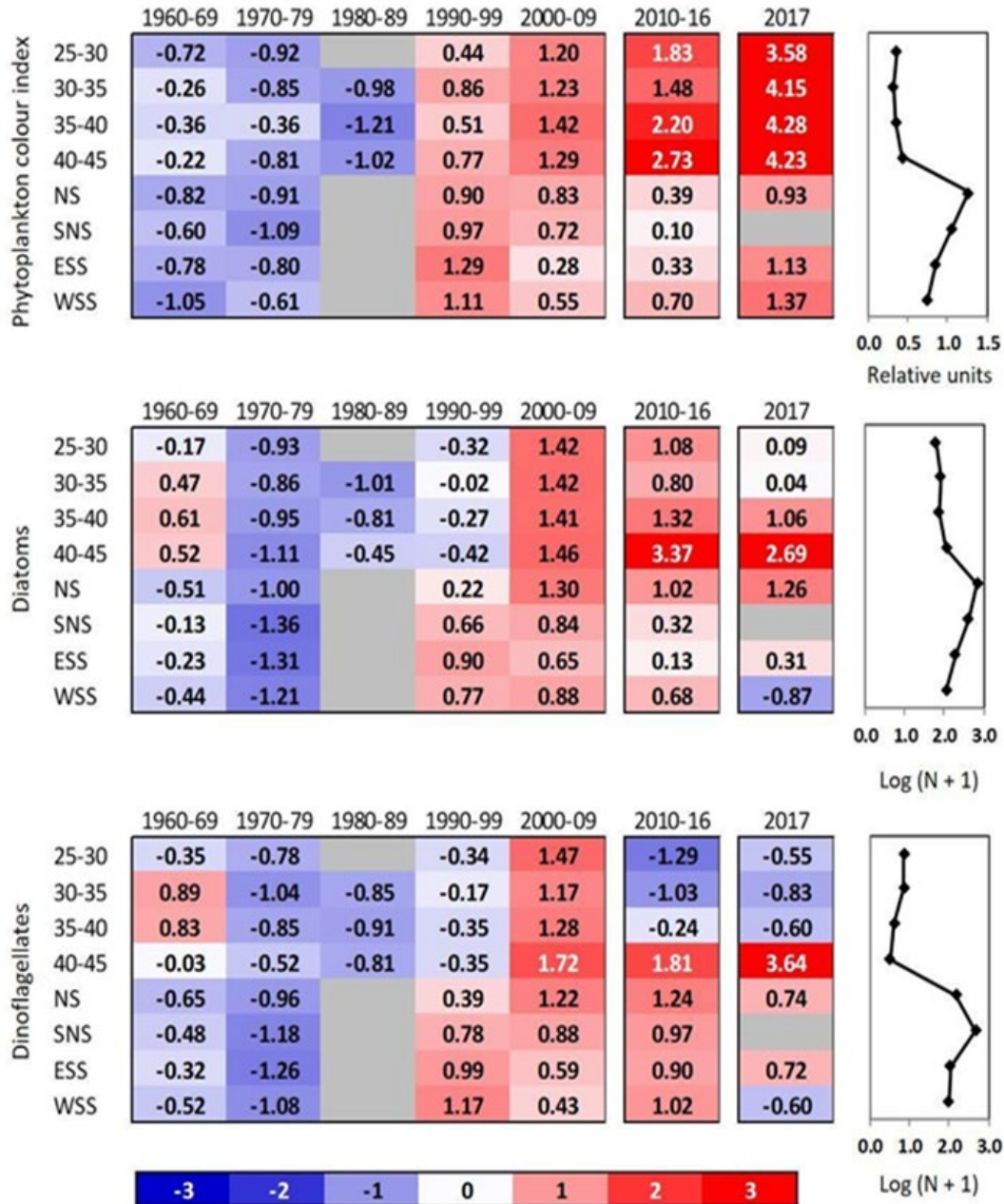


Figure 14. Scorecards for the long-term (1960–2017) Continuous Plankton Recorder (CPR) time series for three indices of phytoplankton concentration in eight regions of the northwest Atlantic. Standardized anomalies were calculated using annual averages calculated from monthly averages over decadal (1960–2009), 7-year (2010–2016), or annual (2017) periods, based on climatological averages calculated for the decadal annual averages between 1960 and 2009 (shown in the panels on the right) and standard deviations calculated for the years 1992–2009. Blank cells correspond to years (decades) when sampling was too sparse to give annual (decadal) values. Red (blue) cells indicate higher-(lower-) than-normal values. The numbers in the cells are the standardized anomalies. The regions are: Western Scotian Shelf (WSS), Eastern Scotian Shelf (ESS), South Newfoundland Shelf (SNS), Newfoundland Shelf (NS), and between longitudes 40–45°W, 35–40°W, 30–35°W, 25–30°W.

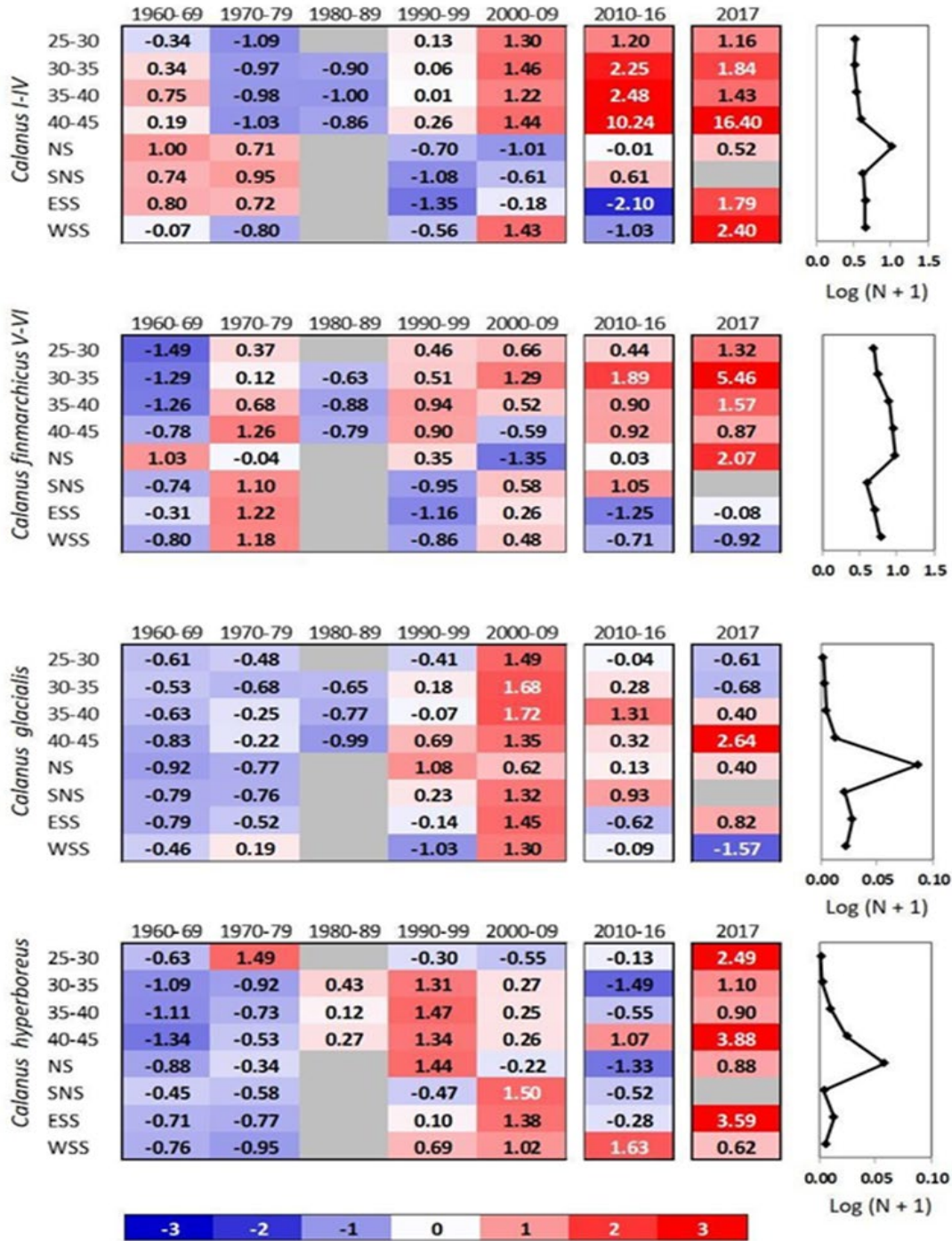


Figure 15. Scorecards for long-term (1960–2016) CPR time series for four *Calanus* taxa in eight regions in the northwest Atlantic. Standardized anomalies were calculated using annual averages calculated from monthly averages over decadal (1960–2009), 7-year (2010–2016), or annual (2017) periods, based on climatological averages calculated for the decadal annual averages between 1960 and 2009 (shown in the panels on the right) and standard deviations calculated for the years 1992–2009. Blank cells correspond to years (decades) when sampling was too sparse to give annual (decadal) values. Red (blue) cells indicate higher-(lower-) than-normal values. The numbers in the cells are the standardized anomalies. The regions are: Western Scotian Shelf (WSS), Eastern Scotian Shelf (ESS), South Newfoundland Shelf (SNS), Newfoundland Shelf (NS), and between longitudes 40–45°W, 35–40°W, 30–35°W, 25–30°W.

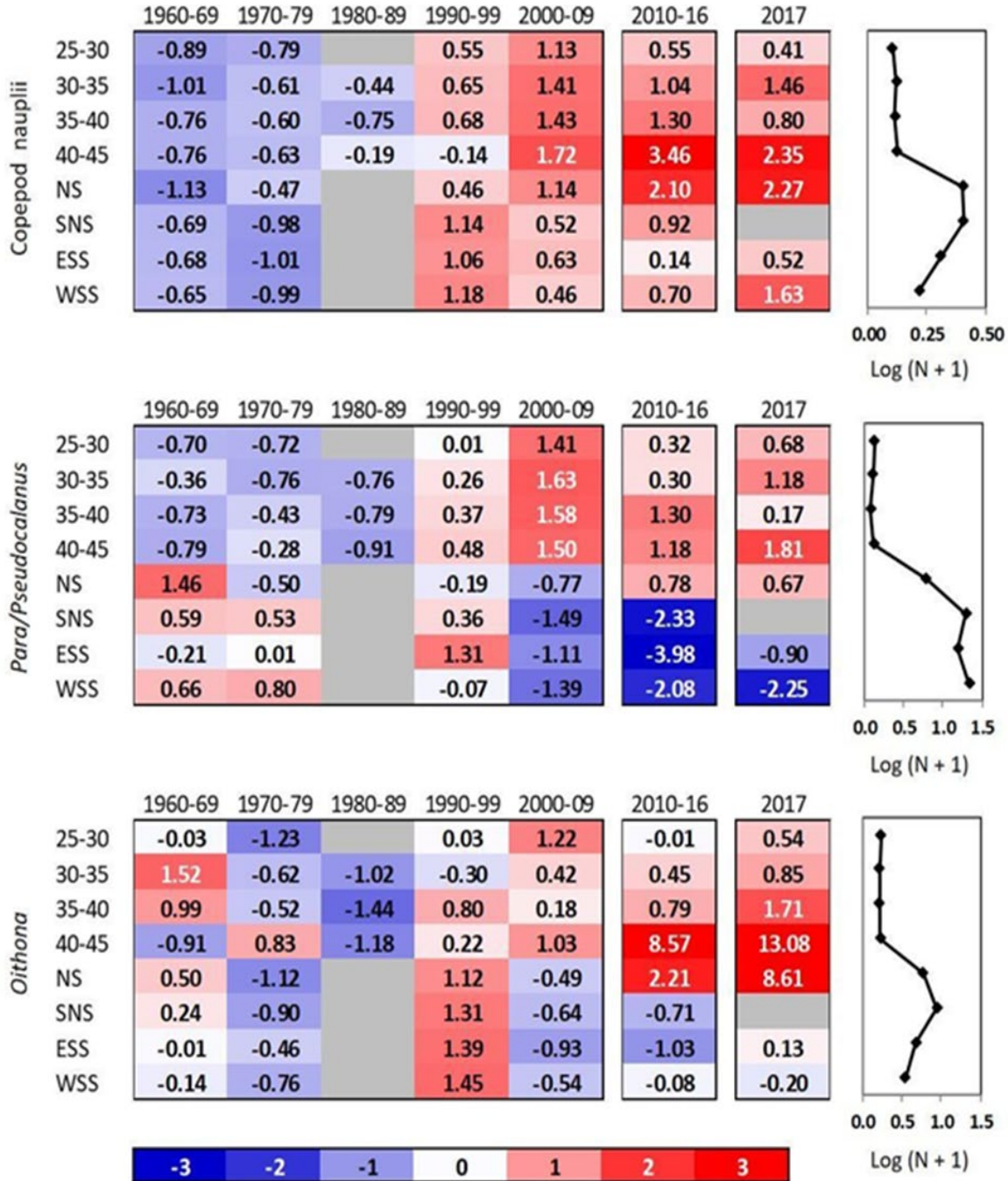


Figure 16. Scorecards for long-term (1960–2017) CPR time series for three small copepod taxa in eight regions in the northwest Atlantic. Standardized anomalies were calculated using annual averages calculated from monthly averages over decadal (1960–2009), 7-year (2010–2016), or annual (2017) periods, based on climatological averages calculated for the decadal annual averages between 1960 and 2009 (shown in the panels on the right) and standard deviations calculated for the years 1992–2009. Blank cells correspond to years (decades) when sampling was too sparse to give annual (decadal) values. Red (blue) cells indicate higher-(lower-) than-normal values. The numbers in the cells are the standardized anomalies. The regions are: Western Scotian Shelf (WSS), Eastern Scotian Shelf (ESS), South Newfoundland Shelf (SNS), Newfoundland Shelf (NS), and between longitudes 40–45°W, 35–40°W, 30–35°W, 25–30°W.

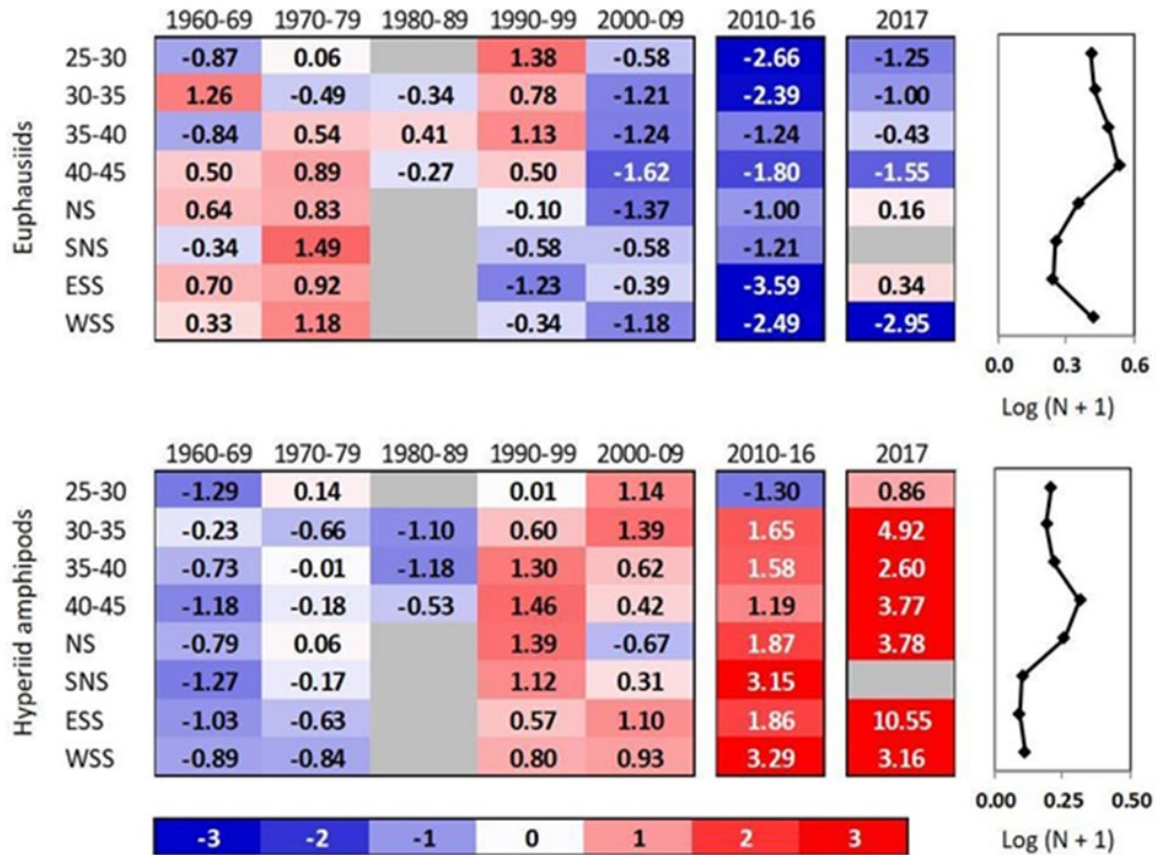


Figure 17. Scorecards for long-term (1960–2017) CPR time series for two macrozooplankton taxa in eight regions in the northwest Atlantic. Standardized anomalies were calculated using annual averages calculated from monthly averages over decadal (1960–2009), 7-year (2010–2016), or annual (2017) periods, based on climatological averages calculated for the decadal annual averages between 1960 and 2009 (shown in the panels on the right) and standard deviations calculated for the years 1992–2009. Blank cells correspond to years (decades) when sampling was too sparse to give annual (decadal) values. Red (blue) cells indicate higher-(lower-) than-normal values. The numbers in the cells are the standardized anomalies. The regions are: Western Scotian Shelf (WSS), Eastern Scotian Shelf (ESS), South Newfoundland Shelf (SNS), Newfoundland Shelf (NS), and between longitudes 40–45°W, 35–40°W, 30–35°W, 25–30°W.

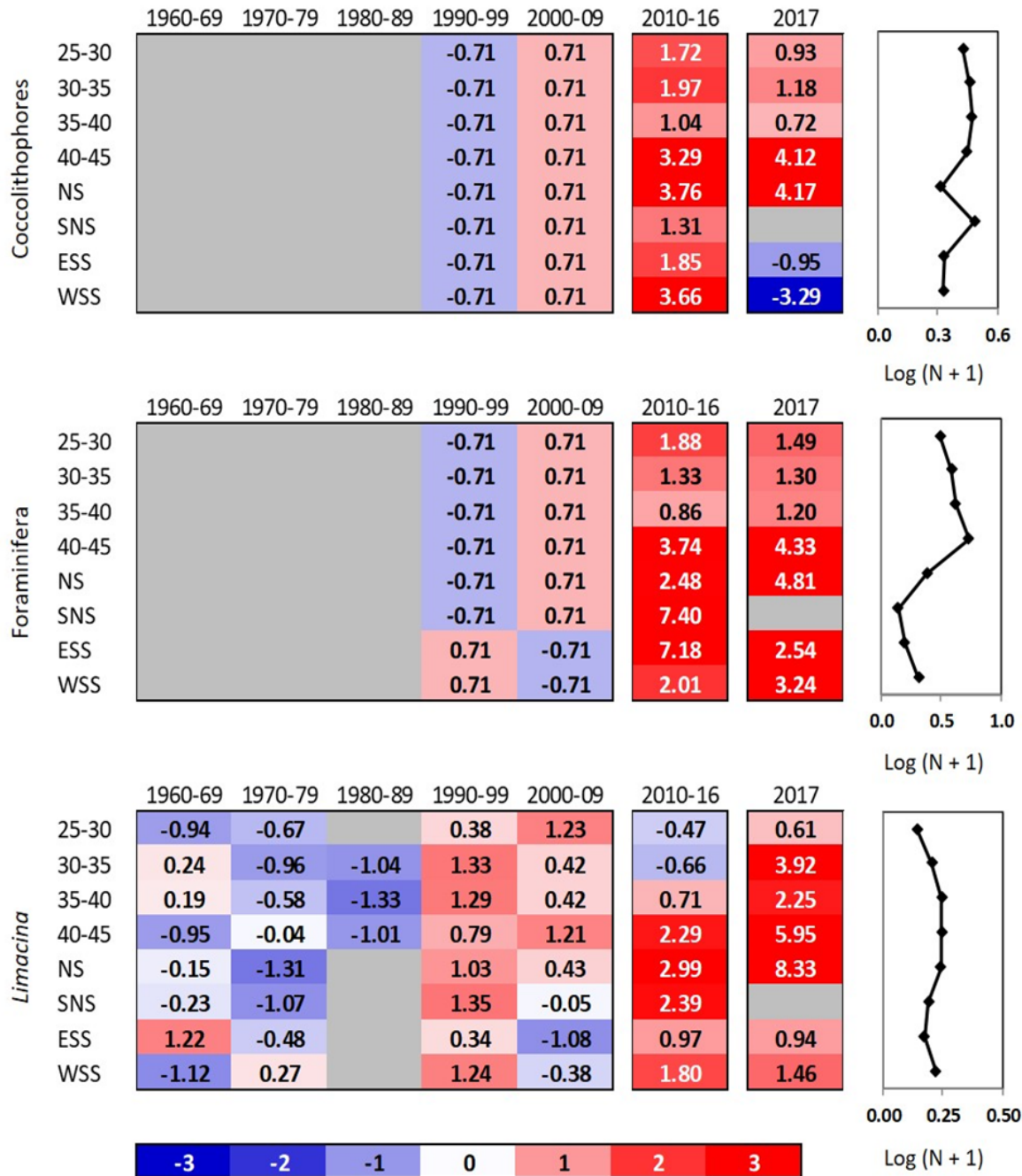


Figure 18. Scorecards for long-term (1960–2017) CPR time series for acid-sensitive taxa in eight regions in the northwest Atlantic. Standardized anomalies were calculated using annual averages calculated from monthly averages over decadal (1960–2009), 7 year (2010–2016), or annual (2017) periods, based on climatological averages calculated for the decadal annual averages between 1960 and 2009 (shown in the panels on the right) and standard deviations calculated for the years 1992–2009. Blank cells correspond to years (decades) when sampling was too sparse to give annual (decadal) values. Red (blue) cells indicate higher-(lower-) than-normal values. The numbers in the cells are the standardized anomalies. The regions are: Western Scotian Shelf (WSS), Eastern Scotian Shelf (ESS), South Newfoundland Shelf (SNS), Newfoundland Shelf (NS), and between longitudes 40–45°W, 35–40°W, 30–35°W, 25–30°W.

ANNEX 1

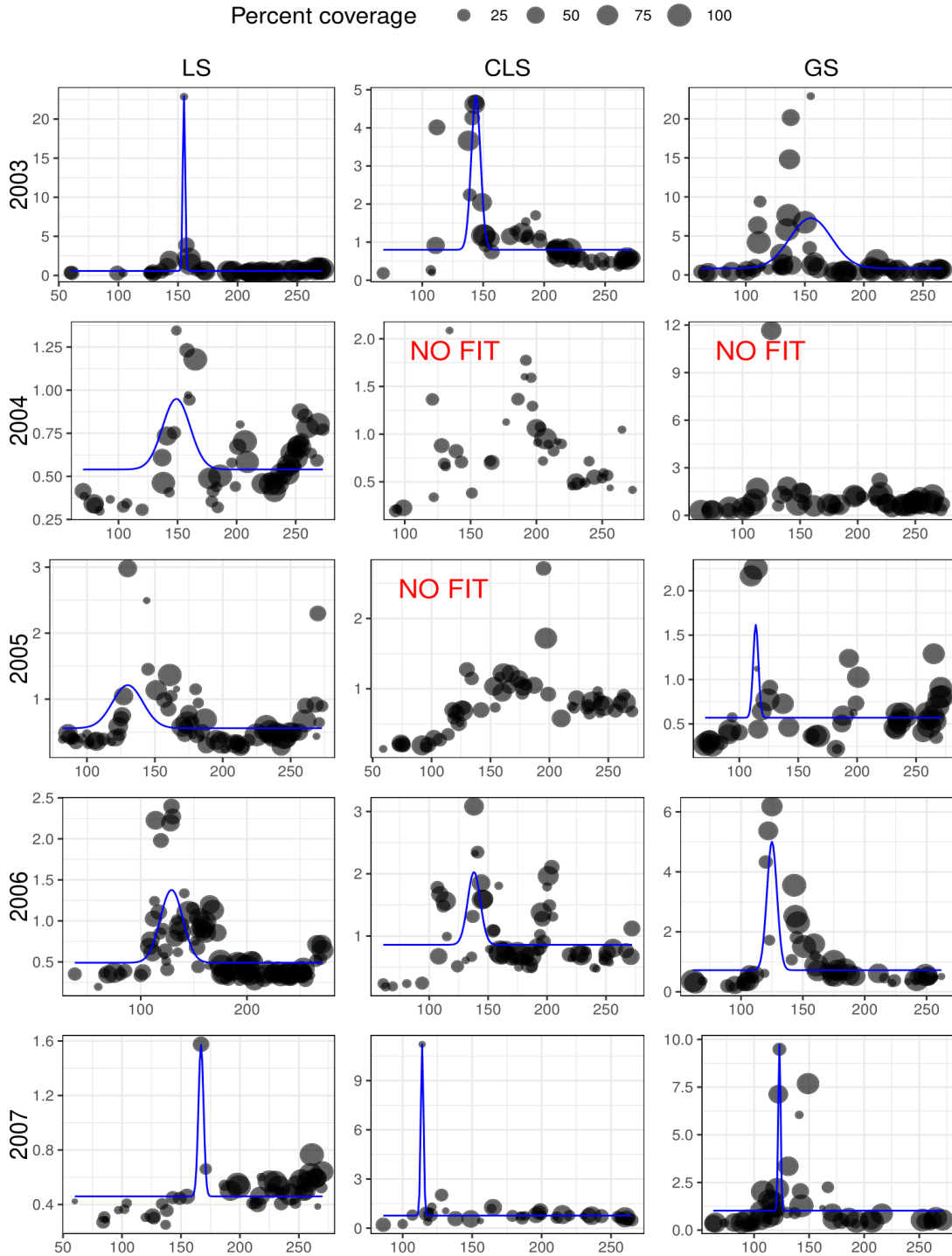


Figure A1. Average daily chlorophyll-a concentration from MODIS-Aqua (solid circles) for the Labrador Shelf, Central Labrador Sea, and Greenland Shelf (columns from left to right respectively) between 2003 and 2007. Blue solid lines correspond to the phytoplankton spring bloom fit using the shifted Gaussian approach. Solid circle size corresponds to the percentage of data available on a given day in the regions..

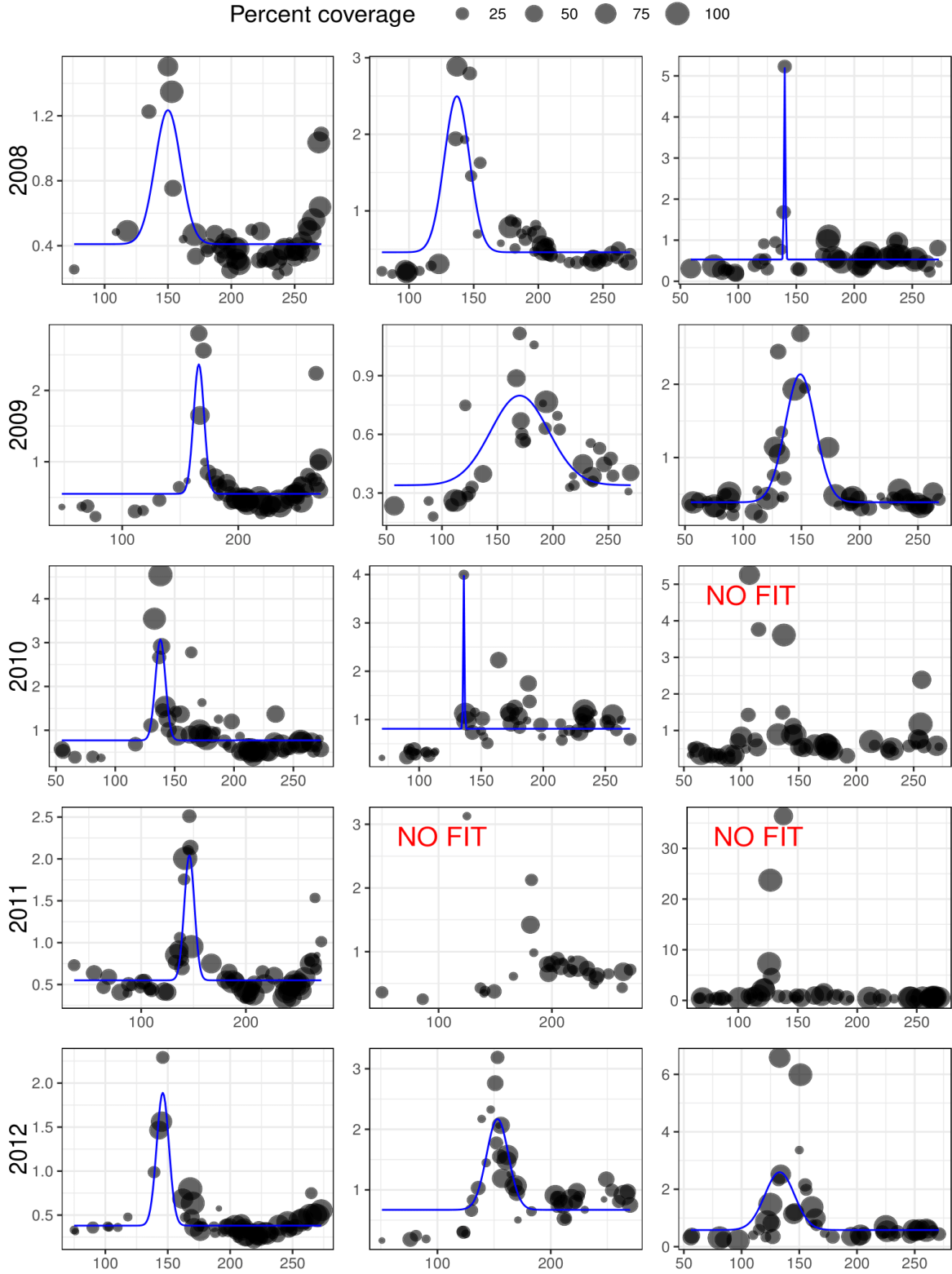


Figure A2. Average daily chlorophyll-a concentration from MODIS-Aqua (solid circles) for the Labrador Shelf, Central Labrador Sea, and Greenland Shelf (columns from left to right, respectively) between 2008 and 2012. Blue solid lines correspond to the phytoplankton spring bloom fit using the shifted Gaussian approach. Solid circle size corresponds to the percentage of data available on a given day in the regions.

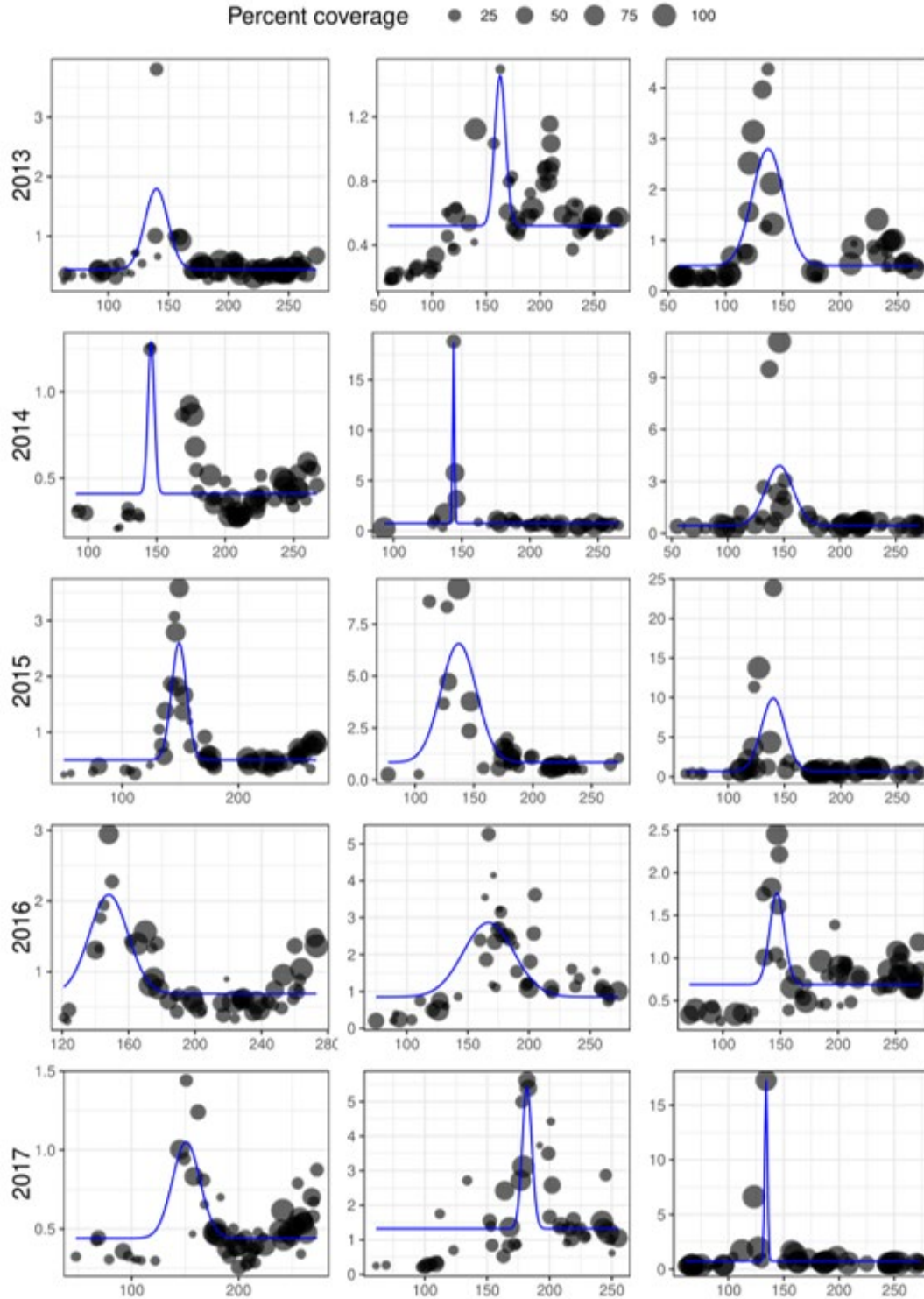


Figure A3. Average daily chlorophyll-a concentration from MODIS-Aqua (solid circles) for the Labrador Shelf, Central Labrador Sea, and Greenland Shelf (columns from left to right, respectively) between 2013 and 2017. Blue solid lines correspond to the phytoplankton spring bloom fit using the shifted Gaussian approach. Solid circle size corresponds to the percentage of data available on a given day in the regions.

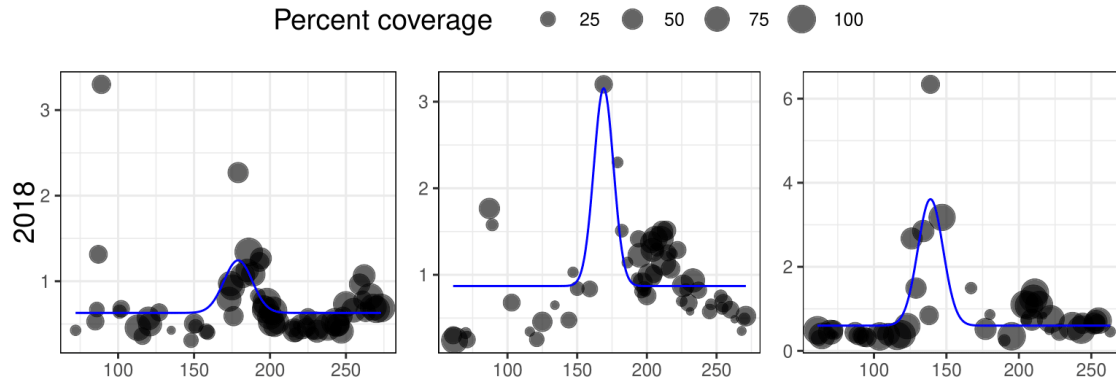


Figure A4. Average daily chlorophyll-a concentration from MODIS-Aqua (solid circles) for the Labrador Shelf, Central Labrador Sea, and Greenland Shelf 2018 (from left to right, respectively). Blue solid lines correspond to the phytoplankton spring bloom fit using the shifted Gaussian approach. Solid circle size corresponds to the percentage of data available on a given day in the regions.